Supporting Information

Luminescent Neutral Cyclometalated Iridium(III) Complexes Featuring a Cubic Polyhedral Oligomeric Silsesquioxane for Lipid Droplet Imaging and Photocytotoxic Applications

Jing-Hui Zhu,[†] Shek-Man Yiu,[†] Ben Zhong Tang,*[,‖] and Kenneth Kam-Wing Lo*[,†,‡,§]

[†]Department of Chemistry, City University of Hong Kong, Tat Chee Avenue, Hong Kong, P. R. China; Email: bhkenlo@cityu.edu.hk

[‡]State Key Laboratory of Terahertz and Millimeter Waves, City University of Hong Kong, Tat Chee Avenue, Hong Kong, P. R. China

[§]Center of Functional Photonics, City University of Hong Kong, Tat Chee Avenue, Hong Kong, P. R. China

[‖]Department of Chemistry, The Hong Kong University of Science and Technology, Clear Water Bay, Kowloon, Hong Kong, P. R. China; Email: tangbenz@ust.hk

Table of Contents

EXPERIMENTAL

Materials and reagents

Aminopropyl heptakis(isobutyl) POSS was obtained from Hybrid Plastics, Inc. Methoxypoly(ethylene glycol) amine ($mPEG_{5k}$-NH_2) was received from JenKem Technology Co. Ltd. Salicylaldehyde (reagent grade, 98%) and 4-aminobenzyl alcohol (purity: 97%) were ordered from Energy Chemical. 4-Nitrophenyl chloroformate (purity: 90%) was acquired from Bide Pharmatech Ltd. Iridium(III) chloride hydrate ($IrCl_3 \cdot xH_2O$) was purchased from Precious Metal Online. Pluronic F127, 2-phenyl pyridine (Hppy), 2-phenyl benzothiazole (Hbt), and triethylamine were purchased from Sigma-Aldrich. The ligand 2-(1-naphthyl)benzothiazole (Hbsn)[1] and the chloro-bridged dimers[2] (including $[Ir(ppy)_2Cl]_2$, $[Ir(bt)_2Cl]_2$, and $[Ir(bsn)_2Cl]_2$) were prepared as reported previously. Unless otherwise stated, all the other chemicals were purchased from commercial suppliers and used without further purification. All solvents were of analytical grade and purified according to standard procedures.[3] Autoclaved Milli-Q water was used for the preparation of the aqueous solutions. Dulbecco's modified Eagle's medium (DMEM), fetal bovine serum (FBS), phosphate-buffered saline (PBS), trypsin-EDTA (0.5%, no phenol red), and penicillin/streptomycin were purchased from Invitrogen.

Synthesis and characterization

Synthesis of *N*-(4-hydroxymethylphenyl)-1-(2-hydroxyphenyl)methanimine (HL1)

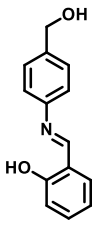

To an ethanol solution (30 mL) of 4-aminobenzyl alcohol (1.23 g, 10 mmol) was added salicylaldehyde (1.22 g, 10 mmol, 1.065 mL). The reaction mixture immediately became dark yellow and was allowed to reflux for 12 h. The resulting mixture was cooled to room temperature and the dark yellow residue was collected by filtration, washed with cold ethanol, then with diethyl ether and dried under vacuum. Yield: (1.99 g, 88%). ^{1}H NMR (300 MHz, DMSO-d_6, 298 K): δ_H/ppm: 13.19 (s, 1H, –OH of phenol), 8.97 (s, 1H, –CH=N–), 7.65 (dd, 1H, J = 7.6, 1.6 Hz, H6 of phenol ring), 7.45 – 7.36 (m, 5H, H2, H3, H5, and H6 of phenyl ring, H4 of phenol ring), 7.01 – 6.93 (m, 2H, H3 and H5 of phenol ring), 5.25 (t, 1H, J = 5.7 Hz, –OH of –CH_2OH), 4.52 (d, 2H, J = 5.7 Hz, –CH_2–). Positive ESI-MS (m/z): 228.2 [M + H^+]$^+$. IR (KBr disk, v/cm^{-1}): 3449 (O–H stretching).

Synthesis of [Ir(ppy)$_2$(L1)] (**1a**)

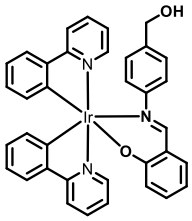

A mixture of [Ir(ppy)$_2$Cl]$_2$ (54 mg, 0.05 mmol), HL1 (22.8 mg, 0.1 mmol), potassium carbonate (41.4 mg, 0.3 mmol) in CH_2Cl_2/MeOH (30 mL, 1:1, v/v) was stirred and heated under reflux for 12 h. The reaction mixture was evaporated to dryness and the resulting yellow solid was dissolved in a minimum amount of CH_2Cl_2. The mixture was filtered and filtrate was evaporated to dryness to give the crude product, which was subsequently purified by column chromatography on silica gel using CH_2Cl_2 as the eluent. The solution containing the product was rotary evaporated to afford a yellow solid. Yield: (41 mg, 57%). ^{1}H NMR (300 MHz, DMSO-d_6, 298 K): δ_H/ppm: 8.90 (d, 1H, J = 5.6 Hz, H6 of pyridyl ring of ppy), 8.67 (d, 1H, J = 5.7 Hz, H6’ of

pyridyl ring of ppy), 8.21 (s, 1H, –CH=N–), 8.15 (d, 1H, *J* = 8.1 Hz, H6 of phenyl ring of ppy), 7.96 – 7.85 (m, 3H, H3 and H3' of pyridyl ring of ppy, H6' of phenyl ring of ppy), 7.71 (d, 1H, *J* = 7.8 Hz, H6 of phenol ring of L1), 7.42 – 7.10 (m, 5H, H4, H4', H5, and H5' of phenyl ring of ppy, and H4 of phenol of L1), 6.79 (t, 1H, *J* = 7.4 Hz, H4 of pyridyl ring of ppy), 6.69 (d, 2H, *J* = 8.2 Hz, H3 and H3' of phenyl ring of ppy), 6.62 (t, 1H, *J* = 7.3 Hz, H4' of pyridyl ring of ppy), 6.46 (dd, 2H, *J* = 14.5, 7.7 Hz, H5 and H5' of pyridyl ring of ppy), 6.41 – 6.27 (m, 2H, H3 and H5 of phenol ring of L1), 6.15 (d, 2H, *J* = 8.2 Hz, H3 and H3' of phenyl ring of L1), 6.03 (1H, d, *J* = 7.4 Hz, H2 of phenyl ring of L1), 5.92 (d, 1H, *J* = 7.4 Hz, H2' of phenyl ring of L1), 5.02 (t, 1H, *J* = 5.6 Hz, –OH of $–CH_2OH$), 4.23 (d, 2H, *J* = 5.6 Hz, $–CH_2–$). Positive-ion ESI-MS (*m/z*): 728.5 $[M + H^+]^+$. Elemental analysis (%) calcd. for $IrC_{36}H_{28}N_3O_2·H_2O$: C, 58.05; H, 4.06; N, 5.64. Found: C, 58.01; H, 4.16; N, 5.39. IR (KBr disk, ν/cm^{-1}): 3446 (O–H stretching).

Synthesis of $[Ir(bt)_2(L1)]$ (**2a**)

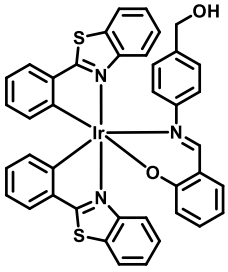

The synthetic procedure was similar to that for complex **1a**, except that $[Ir_2(bt)_4Cl_2]$ (65 mg, 0.05 mmol) was used instead of $[Ir_2(ppy)_4Cl_2]$. Complex **2a** was achieved as an orange solid. Yield: (51 mg, 61 %). ^{1}H NMR (300 MHz, $CDCl_3$, 298 K): δ_H/ppm: 8.64 (d, 1H, *J* = 9.3 Hz, H4 of benzothioazole ring of bt), 8.26 (d, 1H, *J* = 9.4 Hz, H4' of benzothioazole ring of bt), 7.96 (s, 1H, –CH=N–), 7.90 – 7.79 (m, 2H, H6 and H6' of phenyl ring of bt), 7.72 – 7.66 (m, 1H, H6 of phenol ring of L1), 7.45 – 7.30 (m,

4H, H6, H6', H7, and H7' of benzothioazole ring of bt), 7.15 – 7.06 (m, 2H, H5, and H5' of benzothioazole ring of bt), 6.97 (dd, 1H, *J* = 7.9, 1.8 Hz, H5 of phenyl ring of bt), 6.92 – 6.87 (m, 1H, H4 of phenol ring of L1), 6.77 – 6.64 (m, 4H, H3, H3', H4, and H4' of phenyl ring of bt), 6.64 – 6.56 (m, 1H, H5' of phenol ring of bt), 6.56 – 6.49 (m, 1H, H5 of phenyl ring of L1), 6.38 (dd, 2H, *J* = 7.2, 3.7 Hz, H3 of phenol of L1, H3 of phenyl of L1), 6.30 – 6.23 (m, 1H, H3' of phenyl ring of L1), 6.19 (d, 2H, *J* = 8.3 Hz, H2 and H2' of phenyl of L1), 4.47 (d, 2H, *J* = 5.9 Hz, –CH_2–). Positive-ion ESI-MS (m/z): 840.5 $[M + H^+]^+$. Elemental analysis (%) calcd. for $IrC_{40}H_{28}N_3O_2S_2 \cdot H_2O$: C, 56.06; H, 3.53; N, 4.90. Found: C, 56.15; H, 3.45; N, 4.70. IR (KBr disk, ν/cm^{-1}): 3449 (O–H stretching).

Synthesis of $[Ir(bsn)_2(L1)]$ (**3a**)

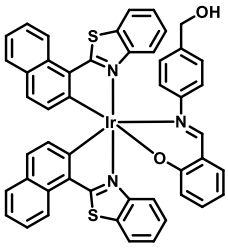

The synthetic procedure was similar to that for complex **1a**, except that $[Ir_2(bsn)_4Cl_2]$ (75 mg, 0.05 mmol) was used instead of $[Ir_2(ppy)_4Cl_2]$. Complex **3a** was obtained as an orange-red solid. Yield: (50 mg, 53 %). ^{1}H NMR (300 MHz, DMSO, 298 K): δ_H/ppm: 8.60 (dd, 2H, *J* = 8.3, 2.7 Hz, H8 and H8' of naphthyl ring of bsn), 8.38 – 8.24 (m, 3H, H4, H4', and H5 of naphthyl ring of bsn), 8.13 (s, 1H, –CH=N–), 8.02 (d, *J* = 8.6 Hz, 1H, H5' of naphthyl ring of bsn), 7.72 (dd, 2H, *J* = 11.8, 6.8 Hz, H4 and H4' of benzothioazole ring of bsn), 7.62 (d, 1H, *J* = 7.9 Hz, H6 of phenol ring of L1), 7.58 – 7.46 (m, 4H, H3 and H3' of naphthyl ring of bsn, H7 and H7' of benzothioazole ring of bsn), 7.41 (dt, 2H, *J* = 11.8, 6.0, 6.0 Hz, H6 and H6' of

benzothioazole ring of bsn), 7.29 (t, 1H, J = 7.2 Hz, H4 of phenol ring of L1), 7.16 (dd, 2H, J = 13.2, 5.1 Hz, H7 and H7' of naphthyl ring of bsn), 7.07 (dd, 2H, J = 12.4, 5.3 Hz, H6 and H6' of naphthyl ring of bsn), 6.47 – 6.32 (m, 5H, H5 and H5' of benzothioazole ring of bsn, H3 and H3' of phenyl ring of L1, H4 of phenol ring of L1), 6.22 (t, 1H, J = 7.0 Hz, H5 of phenol ring of L1), 6.00 (d, 2H, J = 8.3 Hz, H2 and H2' of phenyl ring of L1), 4.82 (t, 1H, J = 5.5 Hz, –OH), 3.82 (d, 2H, J = 3.4 Hz, $–CH_2–$). Positive-ion ESI-MS (m/z): 940.4 $[M + H^+]^+$. Elemental analysis (%) calcd. for $IrC_{48}H_{32}N_3O_2S_2 \cdot H_2O$: C, 60.23; H, 3.58; N, 4.39. Found: C, 60.52; H, 3.79; N, 4.15. IR (KBr disk, ν/cm^{-1}): 3449 (O–H stretching).

Synthesis of $[Ir(ppy)_2(L1\text{-}POSS)]$ (**1**)

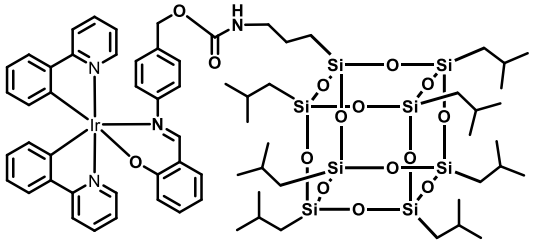

A solution of complex **1a** (73 mg, 0.1 mmol), 4-nitrophenyl chloroformate (20.2 mg, 10 mmol), and triethylamine (200 μL) in CH_2Cl_2 (30 mL) was stirred for 12 h at 298 K. Aminopropyl heptakis(isobutyl) POSS (85 mg, 0.1 mmol) was added and the reaction mixture was vigorously stirred for another 12 h. The resulting solution was evaporated to dryness to give the crude product, which was subsequently purified by column chromatography on silica gel with CH_2Cl_2. The solution containing the product was rotary evaporated to afford complex **1** as a yellow solid. Yield: (107, 66%). ^{1}H NMR (300 MHz, $CDCl_3$, 298 K): δ_H/ppm: 8.86 (dd, 2H, J = 12.6, 5.4 Hz, H6 and H6' of pyridyl ring of ppy), 8.14 (s, 1H, –CH=N–), 7.83 (dd, 2H, J = 8.4, 4.8 Hz, H6 and H6' of phenyl ring of ppy), 7.77 – 7.63 (m, 2H, H3 and H3' of pyridyl

ring of ppy), 7.50 (t, 2H, *J* = 7.9 Hz, H5 and H5' of phenyl ring of ppy), 7.19 – 6.96 (m, 4H, H4 and H4' of phenyl ring of ppy, H4 and H4' of pyridyl ring of ppy), 6.82 – 6.61 (m, 5H, H6 of phenol ring of L1, H3 and H3' of phenyl ring of ppy, H5 and H5' of pyridyl ring of ppy), 6.56 – 6.40 (m, 3H, H3, H4, and H5 of phenol ring of L1), 6.28 (d, 2H, *J* = 7.3 Hz, H3 and H3' of phenyl ring of L1), 6.14 – 6.04 (m, 3H, H2 and H2' of phenyl ring of L1, and –CONH–), 4.84 (s, 2H, $–CH_2O–$), 3.17 (d, 2H, *J* = 6.3 Hz, $–NH–CH_2–$), 1.94 – 1.73 (m, 7H, $–CH(CH_3)_2$), 1.60 – 1.49 (m, 2H, $–CH_2–$), 0.95 (d, 24H, *J* = 6.6 Hz, $–CH_3$), 0.94 (d, 18H, *J* = 6.6 Hz, $–CH_3$), 0.63 – 0.55 (m, 16H, $–CH_2–Si–$). Positive ESI-MS (*m*/*z*): 1627.5 $[M + H^+]^+$. Elemental analysis (%) calcd. for $IrC_{68}H_{97}N_4Si_8O_{15}·2H_2O$: C, 49.10; H, 6.12; N, 3.37. Found: C, 49.04; H, 5.88; N, 3.43. IR (KBr disk, ν/cm^{-1}): 3449 (N–H stretching), 1108 (C–N stretching).

Synthesis of $[Ir(bt)_2(L1\text{-}POSS)]$ (**2**)

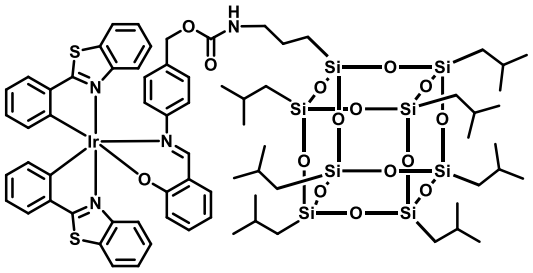

The synthetic procedure was similar to that for complex **1**, except that complex **2a** (84 mg, 0.1 mmol) was used instead of complex **1a**. Complex **2** was obtained as an orange solid. Yield: (109 mg, 63 %). ^{1}H NMR (300 MHz, $CDCl_3$, 298 K): δ_H/ppm: 8.67 – 8.57 (m, 1H, H4 of benzothioazole ring of bt), 8.28 – 8.21 (m, 1H, H4' of benzothioazole ring of bt), 7.97 (s, 1H, –CH=N–), 7.85 (dd, 2H, *J* = 12.0, 5.4 Hz, H6, H6' of phenyl ring of bt), 7.68 – 7.61 (m, 1H, H6 of phenyl ring of L1), 7.44 – 7.30 (m, 4H, H6, H6', H7, and H7' of benzothioazole ring of bt), 7.17 – 7.02 (m, 2H, H5 and H5' of benzothioazole ring of bt), 6.98 (dd, 1H, *J* = 1.7, 7.9 Hz, H5' of phenyl

ring of bt), 6.85 (dd, 1H, J = 10.7, 4.1 Hz, H4' of phenol ring of L1), 6.74 – 6.56 (m, 5H, H3, H3', H4, H4', and H5' of phenyl ring of bt), 6.52 (d, 1H, J = 1.3 Hz, H3 of phenol ring of L1), 6.38 (d, 1H, J = 7.4 Hz, H3 of phenyl ring of L1), 6.36 – 6.25 (m, 2H, H5 of phenol ring of L1, H3' of phenyl ring of L1), 6.17 (d, 2H, J = 8.3 Hz, H2 and H2' of phenyl ring of L1), 4.88 (s, 2H, –CH_2O–), 3.19 (d, 2H, J = 6.5 Hz, –NH–CH_2–), 1.93 – 1.73 (m, 7H, –$CH(CH_3)_2$), 1.61 – 1.53 (m, 2H, –CH_2–), 0.95 (d, 24H, J = 6.6 Hz, –CH_3), 0.94 (d, 18H, J = 6.6 Hz, –CH_3), 0.62 – 0.56 (m, 16H, –CH_2–Si–). Positive-ion ESI-MS (m/z): 1740.4 $[M + H^+]^+$. Elemental analysis (%) calcd. for $IrC_{72}H_{97}N_4Si_8O_{15}S_2 \cdot 3H_2O$: C, 48.21; H, 5.79; N, 3.12. Found: C, 48.37; H, 5.56; N, 2.93. IR (KBr disk, ν/cm^{-1}): 3449 (N–H stretching), 1103 (C–N stretching).

Synthesis of [Ir(bsn)$_2$(L1-POSS)] (**3**)

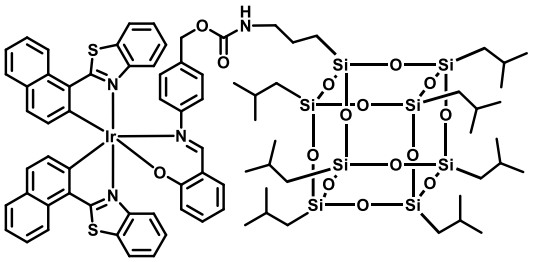

The synthetic procedure was similar to that for complex **1**, except that complex **3a** (94 mg, 0.1 mmol) was used instead of complex **1a**. Complex **3** was obtained as an orange solid. Yield: (105 mg, 57 %). ^{1}H NMR (300 MHz, $CDCl_3$, 298 K): δ_H/ppm: 8.78 (d, 1H, J = 8.7 Hz, H8 of naphthyl ring of bsn), 8.61 (d, 1H, J = 8.5 Hz, H4 of naphthyl ring of bsn), 8.32 (d, 1H, J = 9.0 Hz, H8' of naphthyl ring of bsn), 8.08 (d, 1H, J = 8.5 Hz, H4' of naphthyl ring of bsn), 8.00 – 7.86 (m, 3H, H5, H5' of naphthyl ring of bsn, –CH=N–), 7.66 – 7.53 (m, 3H, H4, H4' of benzothiazole ring of bsn, H3 of naphthyl ring of bsn), 7.48 – 7.27 (m, 7H, H3', H7, H7' of naphthyl ring of bsn, H6, H6' H7, H7' of benzothiazole ring of bsn,), 7.25 – 7.20 (m, 1H, H6 of phenol ring of L1), 7.02

– 7.16 (m, 2H, H6 and H6’ of naphthyl ring of bsn), 6.99 – 6.88 (m, 2H, H4 phenol ring of L1, –NHCO–), 6.62 (d, 2H, *J* = 8.5, H5, H5’ of benzothiazole ring of bsn), 6.55 (d, 1H, *J* = 8.4 Hz, H3 of phenol of L1), 6.43 (d, 2H, *J* = 8.4 Hz, H2, H3 of phenyl of L1), 6.25 (t, 1H, *J* = 6.9 Hz, H5 phenol of L1), 6.11 (d, 2H, *J* = 8.4 Hz, H2’, H3’ of phenyl of L1), 4.65 – 4.50 (m, 2H, $–CH_2–O–$), 3.22 – 3.06 (m, 2H, $–CH_2–$), 1.93 – 1.68 (m, 7H, $–CH(CH_3)_2$), 1.59 – 1.53 (m, 2H, $–CH_2–$), 0.95 (d, 24H, *J* = 6.6 Hz, $–CH_3$), 0.94 (d, 18H, *J* = 6.6 Hz, $–CH_3$), 0.62 – 0.58 (m, 16H, $–CH_2–Si–$). Positive-ion ESI-MS (m/z): 1840.5 $[M + H^+]^+$. Elemental analysis (%) calcd. for $IrC_{80}H_{101}N_4Si_8O_{15}S_2·4H_2O$: C, 50.26; H, 5.75; N, 2.93. Found: C, 50.12; H, 6.16; N, 2.78. IR (KBr disk, ν/cm^{-1}): 3449 (N–H stretching), 1107 (C–N stretching).

Synthesis of $[Ir(ppy)_2(L1\text{-}mPEG_{5K})]$ (**1b**)

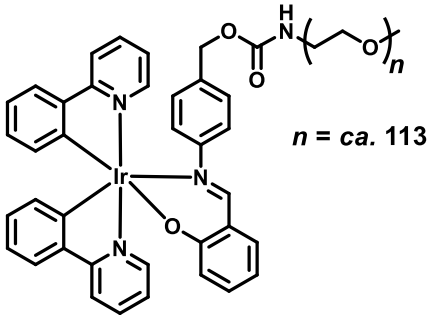

The synthetic procedure was similar to that for complex **1**, except that $mPEG_{5K}\text{-}NH_2$ (500 mg, 0.1 mmol) was used instead of aminopropyl heptakis(isobutyl) POSS. Complex **1b** was obtained as a yellow solid. Yield: (195 mg, 34%). ^1H NMR (300 MHz, $CDCl_3$, 298 K): δ_H/ppm: 8.90 (d, 2H, *J* = 5.0 Hz, H6 and H6’ of pyridyl ring of ppy), 8.11 (s, 1H, –CH=N–), 7.89 (d, 1H, *J* = 7.9 Hz, H6 of phenyl ring of ppy), 7.78 – 7.64 (m, 2H, H3 and H3’ of pyridyl ring of ppy), 7.60 (d, 1H, *J* = 5.0 Hz, H6 of phenol ring of L1), 7.54 (d, 1H, *J* = 8.1 Hz, H6 of phenyl ring of ppy), 7.27 – 7.20 (m, 1H, H4 of phenol ring of L1), 7.18 – 7.09 (m, 2H, H4 and H4’ of phenyl ring of ppy),

7.09 – 6.97 (m, 2H, H5 and H5’ of phenyl ring of ppy), 6.86 (td, 1H, J = 7.6, 1.2 Hz, H4 of pyridyl of ppy), 6.77 – 6.66 (m, 4H, H4’ and H5, of pyridyl ring of ppy, H3 and H3’ of phenyl ring of ppy), 6.57 – 6.38 (m, 3H, H5, of pyridyl ring of ppy, H3 and H5 of phenol ring of L1), 6.28 (d, 1H, J = 6.7 Hz, H3 of phenyl ring of L1), 6.16 – 6.05 (m, 3H, H2, H2’, and H3’ of phenyl ring of L1), 4.84 (s, 2H, –CH_2OOC–), 3.39 (s, 3H, –OCH_3 of PEG). IR (KBr disk, v/cm^{-1}): 3449 (N–H stretching), 1109 (C–N stretching). HPLC (C18, mobile phase: MeOH, flow rate: 4.0 mL min^{-1}): t_R = 7.35 min.

Synthesis of [Ir(bt)$_2$(L1-mPEG$_{5K}$)] (**2b**)

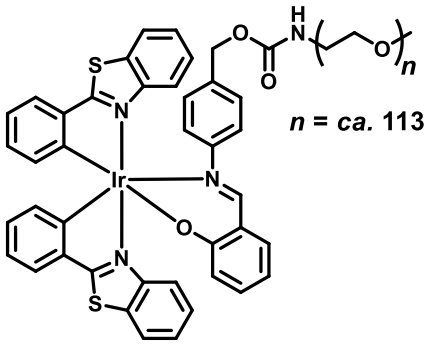

The synthetic procedure was similar to that for complex **2**, except that mPEG$_{5K}$-NH_2 (500 mg, 0.1 mmol) was used instead of aminopropyl heptakis(isobutyl) POSS. Complex **2b** was obtained as an orange solid. Yield: (181 mg, 31%). ^{1}H NMR (300 MHz, $CDCl_3$, 298 K): δ_H/ppm: 8.70 – 8.63 (m, 1H, H4 of benzothioazole ring of bt), 8.26 (dd, 1H, J = 6.4, 2.9 Hz, H4’ of benzothioazole ring of bt), 7.95 (s, 1H, –CH=N–), 7.91 – 7.80 (m, 2H, H6 and H6’ of phenyl ring of bt), 7.74 – 7.67 (m, 1H, H6 of phenol ring of L1), 7.47 – 7.32 (m, 4H, H6, H6’, H7, and H7’ of benzothioazole ring of bt), 7.12 (dd, 1H, J = 6.9, 1.7 Hz, H5 of benzothioazole ring of bt), 7.09 (d, 1H, J = 5.0 Hz, H5 of phenyl ring of bt), 6.98 (dd, 1H, J = 7.9, 1.8 Hz, H5’ of benzothioazole ring of bt), 6.94 – 6.84 (m, 1H, H5’ of phenyl ring of bt), 6.74

– 6.59 (m, 5H, H4 of phenol ring of L1, H3, H3', H4, and H4' of phenyl ring of bt), 6.54 (td, 1H, J = 7.4, 1.4 Hz, H5 of phenol ring of L1), 6.39 (t, 2H, J = 7.2 Hz, H3 of phenol ring of L1, H3 of phenyl ring of L1), 6.26 (dd, 1H, J = 10.7, 3.9 Hz, H3' of phenyl of L1), 6.18 (d, 2H, J = 8.3 Hz, H2 and H2' of phenyl of L1), 4.91 (s, 2H, –CH_2OOC–), 3.40 (s, 3H, –OCH_3). IR (KBr disk, ν/cm^{-1}): 3449 (N–H stretching), 1108 (C–N stretching). HPLC (C18, mobile phase: MeOH, flow rate: 4.0 mL min^{-1}): t_R = 7.73 min.

Synthesis of [Ir(bsn)$_2$(L1-mPEG$_{5K}$)] (**3b**)

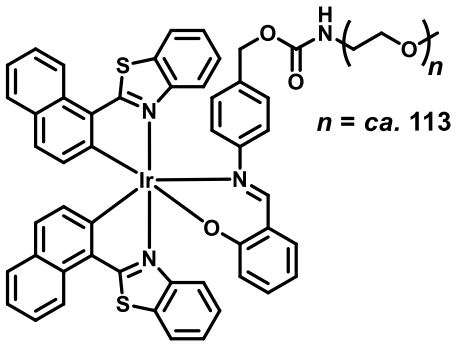

The synthetic procedure was similar to that for complex **3**, except that mPEG$_{5K}$-NH_2 (500 mg, 0.1 mmol) was used instead of aminopropyl heptakis(isobutyl) POSS. Complex **3b** was obtained as an orange-red solid. Yield: (195 mg, 33%). ^{1}H NMR (300 MHz, $CDCl_3$, 298 K): δ_H/ppm: 8.80 (d, 1H, J = 7.7 Hz, H8 of naphthyl ring of bsn), 8.64 (d, 1H, J = 8.5 Hz, H4 of naphthyl ring of bsn), 8.39 – 8.27 (d, 1H, J = 7.5 Hz, H8' of naphthyl ring of bsn), 8.08 (d, 1H, J = 8.6 Hz, H4' of naphthyl ring of bsn), 8.04 – 7.89 (m, 3H, H5, H5' of naphthyl ring of bsn, –CH=N–), 7.73 – 7.52 (m, 3H, H4 and H4' of benzothiazole ring of bsn, H6 of phenol ring of L1), 7.50 – 7.29 (m, 8H, H3, H3', H7 of naphthyl ring of bsn, H6, H6', H7, and H7' of benzothiazole ring of bsn, H4 of phenol of L1), 7.13 – 7.01 (m, 2H, H3 of phenol of L1, –CONH–), 6.96 (dd, 2H, J = 8.2, 5.1 Hz, H7' of naphthyl ring of bsn, H6 of naphthyl of bsn), 6.63 (dd,

2H, J = 8.5, 2.8 Hz, H6’ of naphthyl ring of bsn, H5 of benzothiazole ring of bsn), 6.56 (d, 1H, J = 8.4 Hz, H5’ of benzothiazole ring of bsn), 6.44 (d, 2H, J = 8.3 Hz, H2 and H3 of phenyl ring of L1), 6.26 (t, 1H, J = 6.9 Hz, H5 phenol ring of L1), 6.10 (d, 2H, J = 8.7 Hz, H2’ and H3’ of phenyl ring of L1), 4.66 – 4.38 (m, 2H, –CH_2OOC–), 3.40 (s, 3H, –OCH_3 of PEG). IR (KBr disk, ν/cm^{-1}): 3449 (N–H stretching), 1107 (C–N stretching). HPLC (C18, mobile phase: MeOH, flow rate: 4.0 mL min^{-1}): t_R = 8.08 min.

X-ray crystallography

Single-X-ray data were collected on a Single Crystal X-Ray Diffractometer (Bruker D8 Venture Photon II), using Mo Kα, radiation (0.71073 Å). Data collection was done using *APEX3* v2018.7-2 (Bruker-AXS, 2018) program. Cell refinement and data reduction was done using SAINT V8.38A (Bruker AXS Inc., 2017) program. The structure was solved using *SHELXT* 2014/5 (Sheldrick, 2014) program and refined by *SHELXL* 2016/6 (Sheldrick, 2016) program. All e.s.d.’s (except the e.s.d. in the dihedral angle between two least-squares planes) were estimated using full covariance matrix. Dichloromethane solvent molecules were found to co-crystallize and diffuse in the lattice. The corresponding electron density was treated by PLATON/SQUEEZE procedure and the solvent molecules were omitted in the final model. The X-ray crystallographic data for complex **2a** have been deposited at the Cambridge Crystallographic Data Center (CCDC), under the deposition number CCDC 2085052. The data can be obtained free of charge from the Cambridge Crystallographic Data Center via www.ccdc.cam.ac.uk/data_request/cif

Preparation of Pluronic F127 micelles containing the POSS complexes

Polymeric micelles were fabricated by the solid dispersion methods with slight modification, which involved a cosolubilization-evaporation-dispersion process of a mixture of hydrophobic ingredients and polymeric carriers.[4] The iridium(III) POSS complexes **1** – **3** (*ca.* 2 mg) and Pluronic F127 (PF127, 100 mg) were dissolved in a minimal amount of CH_2Cl_2 (*ca.* 5 mL). The solvent was removed by rotary evaporation. The obtained slurry was redissolved in phosphate-buffered saline (pH 7.4, 10 mM, 10 mL) with the assistance of ultrasonication at 298 K (160 W) for 15 min. An optically transparent and chemically stable micellar solution containing the iridium(III) POSS complexes was yielded, which was subjected to membrane filtration through a 0.2 μm syringe filter. The final concentration of the micellar solution was evaluated on the basis of the iridium(III) POSS complexes.

Dynamical Light Scattering (DLS) measurements

The DLS methodology followed recommendations outlined in the NIST-protocol.[5] The measurements were performed at 298 K using a Dynamic Light Scattering Particle Size Analyzer (Malvem Zetasizer Nano ZS). The results were presented as number-based distributions.

Determination of luminescence quantum yields (Φ_{em})

Luminescence quantum yields were measured by the optically dilute method[6] using an aerated aqueous solution of $[Ru(bpy)_3]Cl_2$ (Φ_{em} = 0.04)[7] as the standard solution.

Determination of singlet oxygen generation quantum yields (Φ_Δ)

The $^1O_2$ production was verified by detecting the photooxidation of 1,3-diphenylisobenzofuran (DPBF) by absorbance measurements versus the irradiation time.[8] The irreversible interaction of DPBF with $^1O_2$ leads to a decrease in 4 the absorbance of the DPBF at *ca*. 418 nm as a consequence of the 1,4-cycloaddition reaction. Stock solutions of all the compounds, $[Ru(bpy)_3]Cl_2$, and DPBF were freshly prepared in CH_3CN. Air-equilibrated CH_3CN solutions containing the iridium(III) complex or the standard (with an absorbance at the excitation wavelength adjusted to 0.15) and DPBF (10 μM) were excited at 450 nm using a Xenon lamp (Ushio) (150 W) with a bandwidth at 20 nm. The decrease of the absorbance caused by photobleaching of DPBF was measured and corrected in all experiments. $[Ru(bpy)_3]Cl_2$ was used as a reference for $^1O_2$ sensitization (Φ_Δ = 0.57 in air equilibrated CH_3CN).[9] The following equation was used for the calculation of Φ_Δ,

$$\phi_{\Delta,\mathrm{s}} = \phi_{\Delta,\mathrm{s}} \times \frac{\mathrm{M_s}}{\mathrm{M_{ref}}} \times \frac{F_{ref}}{F_s}$$

where M is the slope of a linear fit of the change of absorbance at 418 nm against the irradiation time (s) and F is the absorption correction factor, which is given by $F = 1 - 10^{-AL}$ (A = absorbance at 450 nm and L = path length of the cell).

Determination of lipophilicity

Lipophilicity was presented as log $P_{o/w}$ values, which were determined using the flask-shaking method. An aliquot of stock solution of the iridium(III) complex in an aqueous 0.9% NaCl solution (*w*/*v*, saturated with 1-octanol) was added to an equal volume of 1-octanol (saturated with 0.9% *w*/*v* NaCl) and shaken for 2 h at 60 rpm to allow partition at 298 K. After the sample was centrifuged at 14,500 rpm for 15 min,

both layers were carefully separated for iridium analysis. The concentration of iridium-193 in the aqueous phase ($[Ir]_w$) and organic phase ($[Ir]_o$) was determined with a NexION 2000 ICP mass spectrometer (ICP-MS, PerkinElmer SCIEX Instruments, USA) equipped with a peristaltic pump, Meinhard quartz nebulizer, cyclonic spray chamber, nickel skimmer, and sample cones. The partition coefficient ($P_{o/w}$) for each complex was calculated as the ratio $[Ir]_o/[Ir]_w$.

Cell cultures

Human cervical cancer cells (HeLa), human breast cancer cells (MCF-7, estrogen/progesterone (ER/PR) receptor-negative and human epidermal growth factor receptor 2 (HER2) positive), triple-negative human breast cancer cells (MDA-MB-231), human hepatocyte carcinoma cells (HepG2), human lung adenocarcinoma cell line (A549), mouse neuroblastoma cell line (Neuro-2a), human embryonic kidney cells (HEK293T), human foetal lung Cells (MRC-9), and mouse embryonic fibroblast cells (3T3-L1) were used in the present study. All the cell lines were cultured in DMEM containing 10% FBS and 1% antibiotic-antimycotic (penicillin-streptomycin) in an incubator at 37°C under 5% CO_2 atmosphere. For MCF-7 cells, human recombinant insulin (10 μg mL^{-1}) was added to afford a complete growth medium.[10] Cells were subcultured by digesting from the adherent state with 0.25% trypsin in PBS (pH 7.4) to retain their viability when they reached 90% confluence.

Differentiation of 3T3-L1 preadipocytes

3T3-L1 preadipocytes were cultured in DMEM containing 10% FBS and 1% penicillin/streptomycin in an incubator at 37°C under 5% CO_2 atmosphere. At 80%

confluence, cells were induced to differentiate with DMEM supplemented with 10% FBS, and adipogenic hormonal cocktails (0.5 mM of 3-isobutyl-1-methyl xanthine (IBMX), 1 μM of dexamethasone, 10 μg mL^{-1} of insulin).[11] After 48 h stimulation, the medium was replaced with fresh DMEM containing 10% FBS and 10 μg mL^{-1} insulin and the cell were incubated for another 48 h. Then, the medium was replaced with fresh DMEM containing 10% FBS every two days until the cells were treated with the iridium(III) complex.

Live-cell confocal microscopy

Cells in growth medium were seeded on a sterilized coverslip in a 35 mm cell-culture dish and grown at 37°C under a 5% CO_2 atmosphere for 48 h. The culture medium was then removed, and the cell layer was washed gently with PBS (1 mL × 3) and incubated with culture medium containing the iridium(III) complex ([Ir] = 10 μM). After incubation for 6 h, the medium was removed and the cell layer was washed gently with PBS (1 mL × 3). The coverslips were mounted on slides for measurements. Imaging was performed with a confocal microscope (Leica TCS SPE) with an excitation wavelength of 405 nm.

Photostability studies

The photostability of complex **3** was determined using a modified method.[12] HeLa cells were stained separately with the iridium(III) complex (10 μM, 1% PF127, 6 h) and the commercial lipid droplet staining dyes Lipid Blue (10 μM, 15 min) and BODIPY 493/503 (10 μM, 15 min) in a similar manner mentioned above. The cells were then imaged by the same confocal microscope, and the samples were scanned 60 times (scan area: 87.3 μm × 87.3 μm). The intensity (*I*) of each LSCM image was

analyzed using an ImageJ software (Fiji). The emission intensity of the first scan (I_o) was defined as 100%.

Determination of cellular uptake by ICP-MS

Cells were grown in a 50 mm tissue culture dish and incubated at 37°C under a 5% CO_2 atmosphere for 48 h. The culture medium was removed and replaced with fresh medium containing the iridium(III) complex at [Ir] = 10 μM. After incubating for 12 h, the medium was removed, and the cell layer was washed gently with PBS (1 mL × 3). The cell layer was then trypsinized and made up to a final volume of 1 mL with PBS. The cell number was counted with a hemocytometer. The harvested cells were digested with 65% HNO_3 (2 mL) at 60°C for 3 h and then diluted with Milli-Q water to a final volume of 10 mL. The concentration of iridium was determined by ICP-MS.

MTT assays

Cytotoxicity assays were conducted in 96-well cell culture plates (SPL Life Science Co., Ltd.). Cells (*ca.* 10,000 per well) were incubated in supplemented culture medium (100 μL) at 37°C under a 5% CO_2 atmosphere for 24 h. The iridium(III) complex were then added to the wells with the range of [Ir] from about 10^{-7} to 10^{-4} M in the growth medium. Wells containing growth medium and cells only were used as blank controls. After the plates were incubated for 48 h, a fresh medium (100 μL) containing 500 μg mL^{-1} of MTT was added to each well. The plates were incubated for another 4 h. Then, the medium was removed and DMSO (200 μL) was added to each well. The absorbance of all the solutions at 570 nm was measured with a SpectraMax iD5 Multi-Mode Microplate Reader (Molecular Devices Corporation,

California). The IC_{50} values of the complexes were evaluated on the basis of percentage cell survival in a dose-dependent manner relative to the controls.

Determination of photocytotoxicity

Cells were prepared using conventional trypsinization procedure with trypsin/EDTA (0.25%) and incubated in flat-bottom 96-well culture plates for cell viability assessment. After being rested for 24 h, cell cultures were washed with PBS to remove the small number of non-adherent dead cells (< 5%) and incubated with fresh culture medium containing iridium(III) complexes at various concentrations (10^{-7} to 10^{-4} M) for 24 h at 37°C under a 5% CO_2 atmosphere, followed by gentle washing with PBS prior to further incubation in phenol red-free medium. The cells were then irradiated at 450 nm for 5 min using a blue light LED lamp (5 mW cm^{-2}) (Shenzhen Puri Materials Technologies Co. Ltd.). After irradiation, the culture medium was replaced with a fresh growth medium for further incubation in the dark for 24 h. The cell viability was assessed using the MTT assay as described above. In the negative control experiment, cells were treated the same except that they were not irradiated.

Determination of intracellular ROS with CellROX™ Deep Red

The intracellular ROS levels were measured by using a fluorogenic probe CellROX™ Deep Red (Invitrogen).[13] After the cells were pre-incubated with complex **3** (10 μM, 12 h) and CellROX™ Deep Red (5 μM, 30 min) at 37°C under a 5% CO_2 atmosphere in the dark, the medium was removed and replaced by phenol red-free medium, and the culture was irradiated at 450 nm for 5 min using a blue light LED lamp (5 mW cm^{-2}). The stained cells were washed thrice with PBS and the coverslip was mounted onto a sterilized glass slide and then imaged using a Leica TCS SPE confocal

microscope. The fluorescence images were taken with an excitation wavelength of 633 nm and an emission wavelength of 650 – 700 nm. Cells treated with CellROX® Deep Red only without irradiation served as a control.

Detection of nucleus morphology changes using DAPI staining

The nucleus morphology changes were detected using DAPI (Invitrogen) staining.[14] After the cells were co-incubated with complex **3** (10 μM, 12 h) at 37°C under a 5% CO_2 atmosphere in the dark, the medium was removed and replaced by phenol red-free medium, and the culture was irradiated at 450 nm for 5 min using a blue light LED lamp (5 mW cm^{-2}). The cells were washed thrice with PBS, fixed with 4% paraformaldehyde in PBS for 15 min, and nuclei were stained by incubation with a 10 μM solution of DAPI in PBS for 15 min. The stained cells were washed thrice with PBS and the coverslip was mounted onto a sterilized glass slide and then imaged using a Leica TCS SPE confocal microscope. The fluorescence images were taken with an excitation wavelength of 405 nm and an emission wavelength of 415 – 495 nm. Cells treated with DAPI only without irradiation served as a control.

Monitoring of the changes of mitochondrial membrane potential

Cells were incubated with complex **3** (10 μM) for 12 h prior to irradiation at 450 nm for 5 min using a blue light LED lamp (5 mW cm^{-2}). The cells were then incubated at 37°C under a 5% CO_2 atmosphere in the dark for 1 h before being stained with tetramethylrhodamine methyl ester[15] (TMRE, Invitrogen, 10 μM) at 37°C for 10 min. The stained cells were washed thrice with PBS and examined immediately using a Leica TCS SPE confocal microscope. The images were taken with an excitation

wavelength of 488 nm and an emission wavelength range of 500 – 550 nm. Cells treated with TMRE only without irradiation served as a control.

Caspase 3/7 activity assays

Cells were incubated with complex **3** (10 μM) for 12 h prior to irradiation at 450 nm for 5 min using a blue light LED lamp (5 mW cm^{-2}). The cells were then supplemented with fresh medium containing a fluorogenic rhodamine-derived caspase 3/7 substrate (Z-DEVD-R110,[16] Invitrogen, 10 μM) and incubated at 37°C under a 5% CO_2 atmosphere in the dark for 1 h. The stained cells were washed thrice with PBS and examined immediately using a Leica TCS SPE confocal microscope. The fluorescence images were taken with an excitation wavelength of 488 nm and an emission wavelength range of 500 – 550 nm. Cells treated with Z-DEVD-R110 only without irradiation served as a control.

Determination of lipid peroxidation

Cells were incubated with complex **3** (10 μM) for 12 h prior to irradiation at 450 nm for 5 min using a blue light LED lamp (5 mW cm^{-2}). The cells were then supplemented with fresh medium containing a lipid peroxidation probe diphenyl-1-pyrenylphosphine[17] (DPPP, Macklin,10 μM) and incubated at 37°C under a 5% CO_2 atmosphere in the dark for 1 h . The stained cells were washed thrice with PBS and examined immediately using a Leica TCS SPE confocal microscope. The fluorescence images were taken with an excitation wavelength of 405 nm and an emission wavelength range of 415 – 495 nm. Cells treated with DPPP only without irradiation served as a control.

Table S1. Crystal data for complex **2a**

Empirical formula	$C_{40}H_{28}IrN_3O_2S_2$
Formula weight	839.02 g/mol
Temperature	238(2) K
Wavelength	0.71073 A
Crystal system, Space group	triclinic, *P*-1
a, Å	11.4266(3)
b, Å	20.4862(6)
c, Å	25.1424(7)
α, deg	108.8880(10)
β, deg	96.5130(10)
γ, deg	105.6030(10)
Volume, Å^3	5232.0(3)
Z, Calculated density	6, 1.652 g/cm^3
Crystal size, mm × mm × mm	0.25 × 0.20 × 0.15
Index ranges	$-12 \le h \le 12$, $-14 \le k \le 14$, $-23 \le l \le 23$
Reflns collected/unique	178421 / 21384 [*R*(int) = 0.0497]
Completeness	99.8%
Data/restraints/param	21384 / 2 / 1335
GOF on F^2	1.029
Final *R* indices [$I > 2\sigma(I)$]	18841 data; $I > 2\sigma(I)$, *R*1 = 0.0265, *wR*2 = 0.0617
	all data, *R*1 = 0.0333, *wR*2 = 0.0651
Largest diff peak and hole, *e* Å^{-3}	1.420 and −1.480

Table S2. Selected bond lengths (Å) and bond angles (°) for complex **2a**

Ir1–N1	2.167(3)	Ir1–N2	2.065(3)
Ir1–N3	2.078(3)	Ir1–C15	2.007(3)
Ir1–C28	2.017(4)	Ir1–O1	2.135(2)
N1–Ir1–N2	83.50(11)	N1–Ir1–N3	102.81(11)
N1–Ir1–C15	94.30(12)	N1–Ir1–C28	177.15(13)
N1–Ir1–O1	87.33(10)	N2–Ir1–N3	172.43(11)
N2–Ir1–C15	79.91(13)	N2–Ir1–C28	94.33(13)
N2–Ir1–O1	98.99(11)	N3–Ir1–C15	95.31(13)
N3–Ir1–C28	79.49(13)	N3–Ir1–O1	85.60(11)
C15–Ir1–C28	87.13(13)	C15–Ir1–O1	177.91(12)
C28–Ir1–O1	91.19(12)		

Table S3. Electronic absorption spectral data of complexes **1** – **3**, **1a** – **3a**, and **1b** – **3b** at 298 K

Complex	Solvent	λ_{abs}/nm (ε/dm^3 mol^{-1} cm^{-1})
1	CH_2Cl_2	256 (61 115), 300 sh (31 695), 340 sh (11 765), 406 (9 310), 474 sh (2 940)
	CH_3CN	252 (52 845), 297 sh (27 145), 338 sh (10 135), 405 (7 880), 474 sh (2 420)
1a	CH_2Cl_2	257 sh (55 930), 305 sh (23 070), 340 sh (9 920), 407 (8 490), 473 sh (2 480)
	CH_3CN	257 sh (57 140), 305 sh (21 855), 341 sh (9 705), 402 (8 780), 473 sh (2 485)
1b	CH_2Cl_2	257 (50 655), 304 sh (22 025), 339 sh (9 535), 404 (7 830), 473 sh (2 750)
	CH_3CN	254 (43 505), 303 sh (18 105), 338 sh (8 145), 403 (6 820), 473 sh (2 175)
2	CH_2Cl_2	255 (45 155), 323 (33 810), 366 sh (9 635), 419 (9 705)
	CH_3CN	251 (40 630), 321 (29 330), 366 sh (7 630), 422 (8 455)
2a	CH_2Cl_2	275 sh (39 140), 322 (31 035), 360 sh (9 650), 423 (9 580)
	CH_3CN	275 sh (36 790), 319 (29 290), 360 sh (9 000), 417 (9 200)
2b	CH_2Cl_2	273 sh (41 540), 310 (32 235), 360 sh (8 140), 421 (7 855)

	CH_3CN	273 sh (39 950), 321 (31 625), 363 sh (9 990), 422 (9 995)
3	CH_2Cl_2	275 sh (75 770), 301 sh (57 450), 343 (42 630), 436 (16 150), 517 (7 880)
	CH_3CN	275 sh (70 810), 301 sh (53 535), 341 (41 215), 433 (15 630), 516 (7 165)
3a	CH_2Cl_2	275 sh (63 980), 301 sh (49 240), 343 (38 590), 435 (14 050), 516 (6 705)
	CH_3CN	273 sh (67 840), 301 sh (47 465), 341 (34 705), 435 (12 775), 516 (5 390)
3b	CH_2Cl_2	275 sh (61 580), 300 sh (48 730), 344 (38 320), 438 (14 480), 517 (6 510)
	CH_3CN	273 sh (58 440), 300 sh (45 450), 341 (36 280), 435 (13 470), 517 (5 850)

Table S4. Singlet oxygen quantum yields ($\Phi_{\triangle}$) of complexes **1** – **3**, **1a** – **3a**, and **1b** – **3b** in aerated CH_3CN

Complex	$\Phi_{\triangle}$[a]
1	0.15
1a	0.15
1b	0.14
2	0.29
2a	0.27
2b	0.26
3	0.86
3a	0.85
3b	0.85

[a] $[Ru(bpy)_2]Cl_2$ was used as a reference ($\Phi_{\triangle}$ = 0.57 in aerated CH_3CN).[7]

Table S5. Lipophilicity (log $P_{o/w}$) and cellular uptake efficiencies of complexes **1** – **3**, **1a** – **3a**, and **1b** – **3b**

Complex	log $P_{o/w}$	Amount of iridium / (fmol/cell)[a]
1	0.86 ± 0.05	0.57 ± 0.04
1a	0.37 ± 0.01	0.65 ± 0.01
1b	−1.15 ± 0.04	0.55 ± 0.03
2	0.88 ± 0.02	0.69 ± 0.06
2a	0.42 ± 0.01	0.83 ± 0.03
2b	−1.03 ± 0.03	0.54 ± 0.05
3	1.08 ± 0.05	0.74 ± 0.02
3a	0.63 ± 0.02	0.87 ± 0.06
3b	−0.95 ± 0.04	0.58 ± 0.03

[a] Amount of iridium of complexes **1** – **3**, **1a** – **3a**, and **1b** – **3b** associated with an average HeLa cell upon incubation with the complexes (10 μM) at 37°C for 12 h, as determined by ICP-MS.

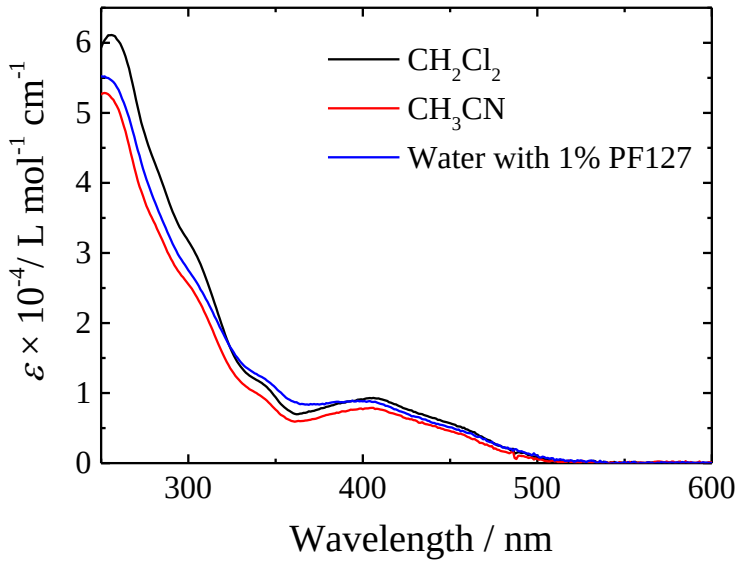

Figure S1. Electronic absorption spectra of complex **1** in CH_2Cl_2 (black) and CH_3CN (red), and water (blue, containing 1% PF127) at 298 K.

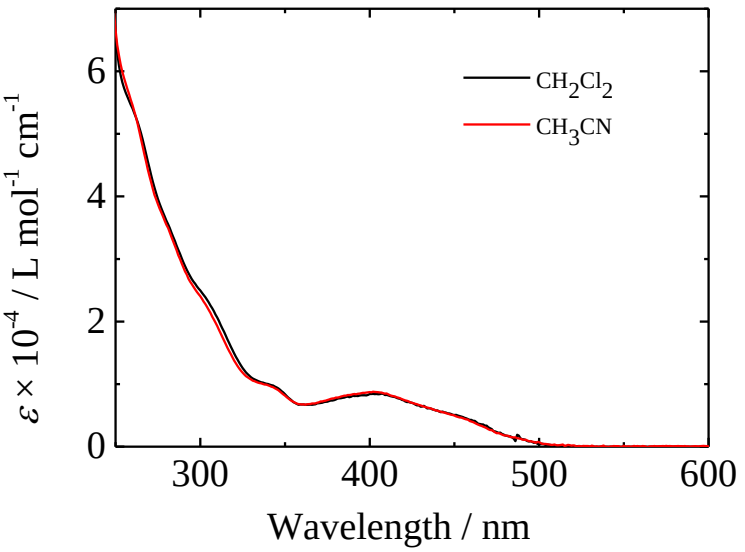

Figure S2. Electronic absorption spectra of complex **1a** in CH_2Cl_2 (black) and CH_3CN (red) at 298 K.

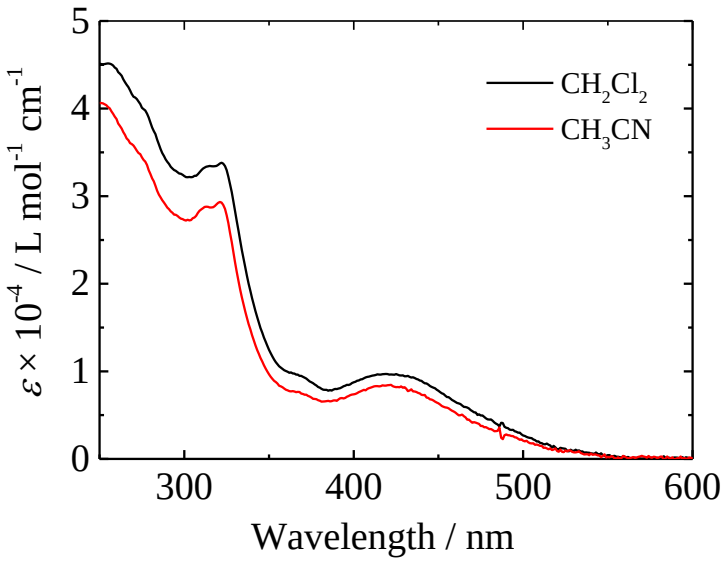

Figure S3. Electronic absorption spectra of complex **1b** in CH_2Cl_2 (black) and CH_3CN (red) at 298 K.

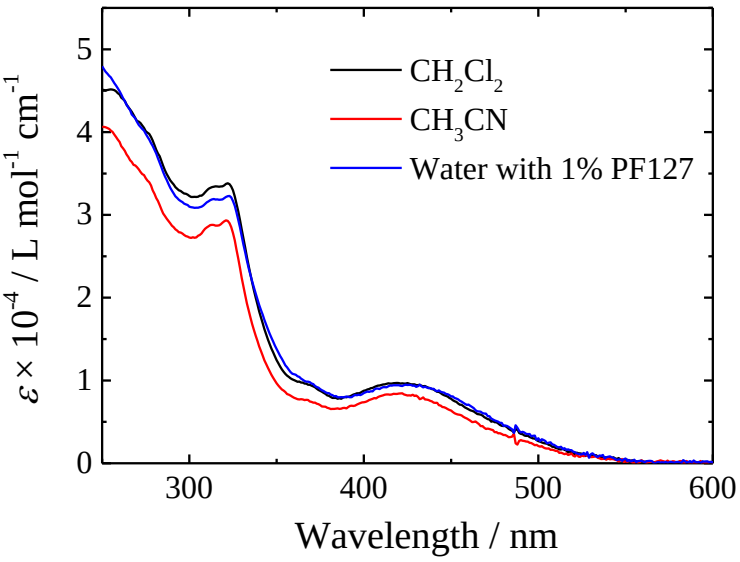

Figure S4. Electronic absorption spectra of complex **2** in CH_2Cl_2 (black) and CH_3CN (red), and water (blue, containing 1% PF127) at 298 K.

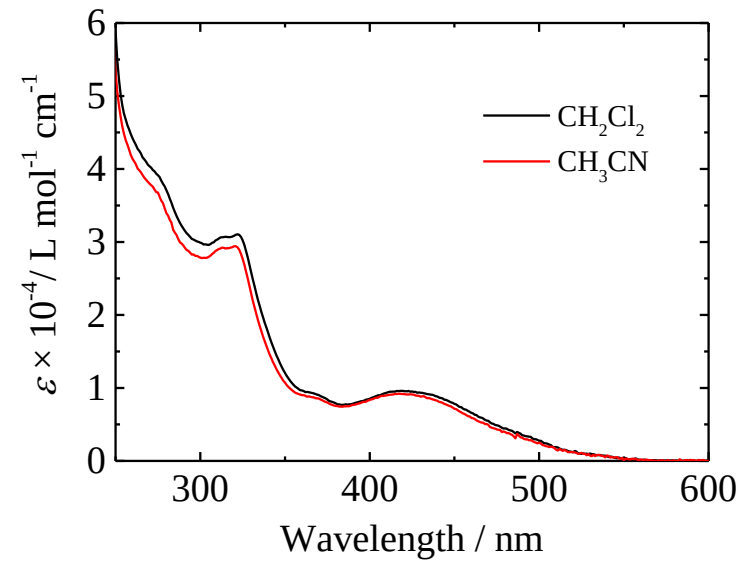

Figure S5. Electronic absorption spectra of complex **2a** in CH_2Cl_2 (black) and CH_3CN (red) at 298 K.

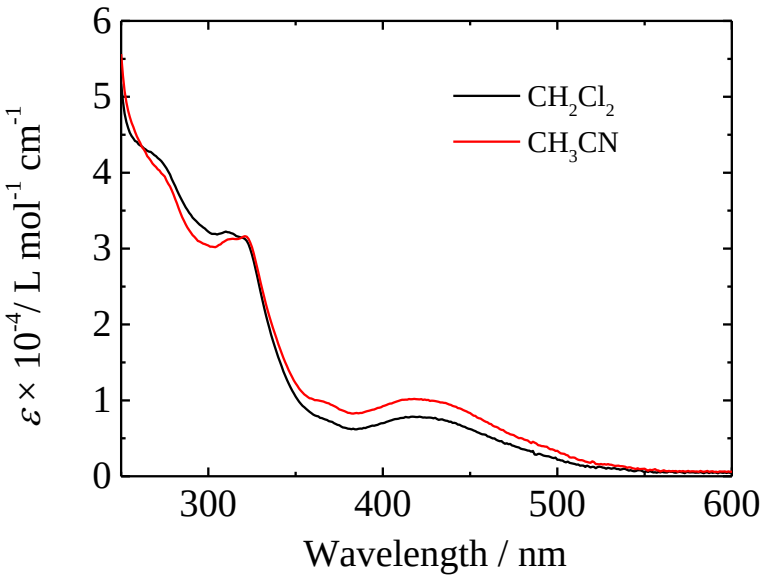

Figure S6. Electronic absorption spectra of complex **2b** in CH_2Cl_2 (black) and CH_3CN (red) at 298 K.

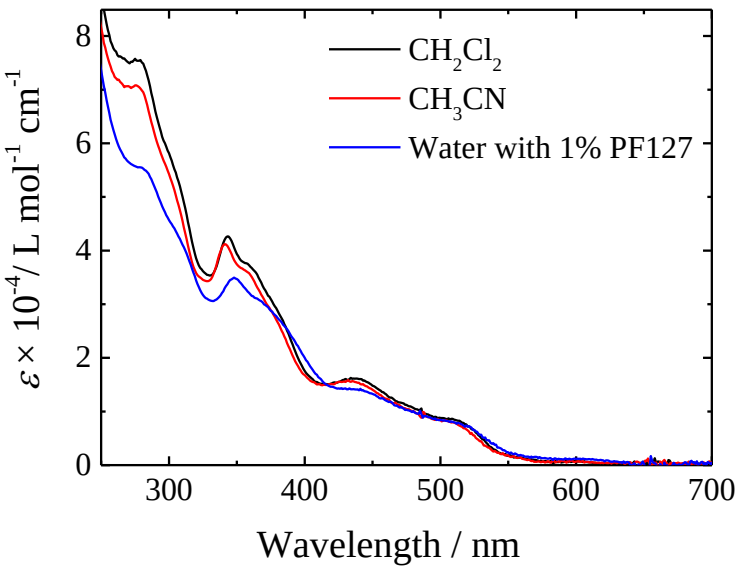

Figure S7. Electronic absorption spectra of complex **3** in CH_2Cl_2 (black) and CH_3CN (red), and water (blue, containing 1% PF127) at 298 K.

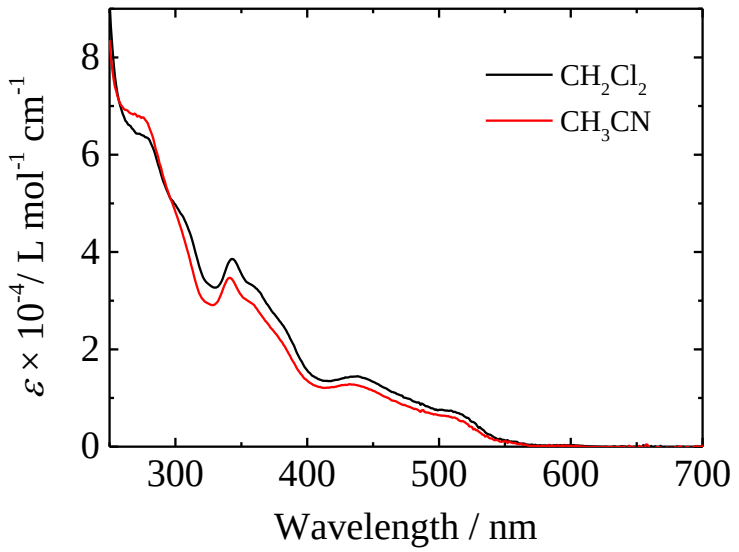

Figure S8. Electronic absorption spectra of complex **3a** in CH_2Cl_2 (black) and CH_3CN (red) at 298 K.

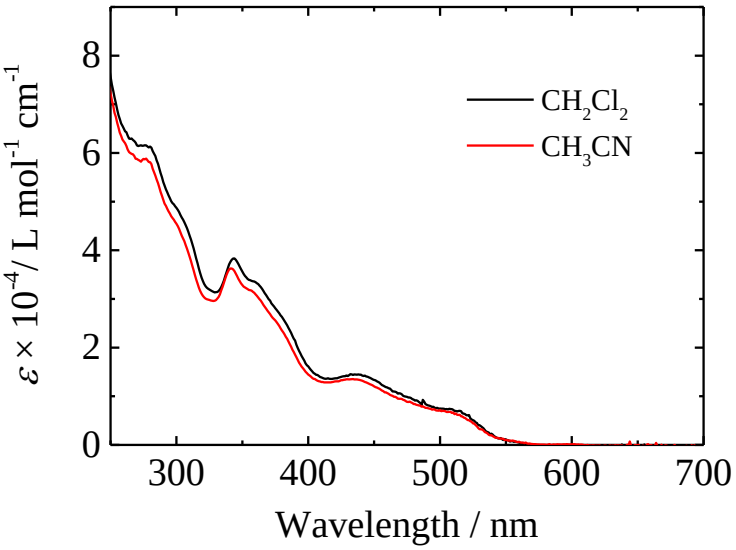

Figure S9. Electronic absorption spectra of complex **3b** in CH_2Cl_2 (black) and CH_3CN (red) at 298 K.

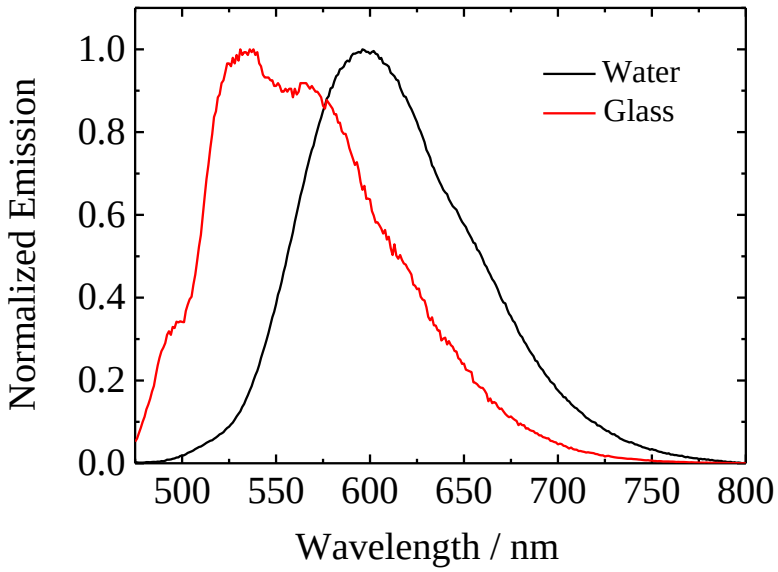

Figure S10. Emission spectra of complex **1** in degassed water (containing 1% PF127) at 298 K (black) and alcoholic glass (EtOH:MeOH = 4:1, *v*/*v*) at 77 K (red).

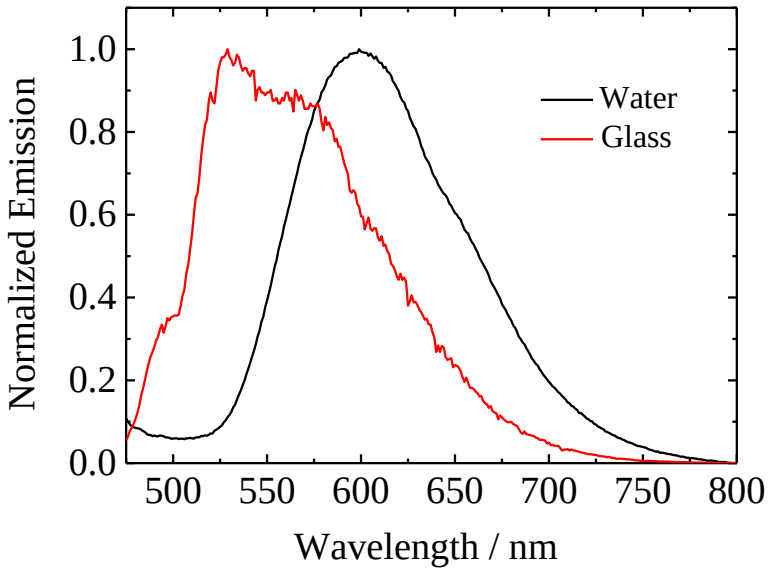

Figure S11. Emission spectra of complex **1a** in degassed water at 298 K (black) and alcoholic glass (EtOH:MeOH = 4:1, *v*/*v*) at 77 K (red).

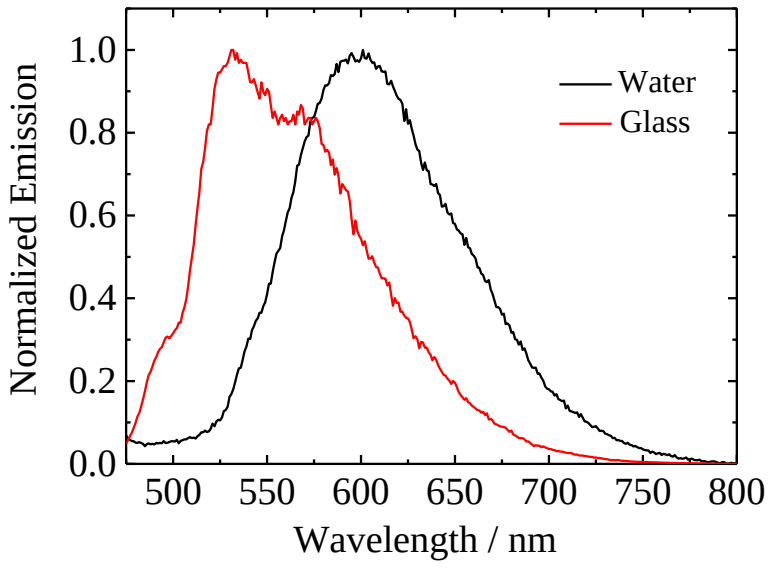

Figure S12. Emission spectra of complex **1b** in degassed water at 298 K (black) and alcoholic glass (EtOH:MeOH = 4:1, *v*/*v*) at 77 K (red).

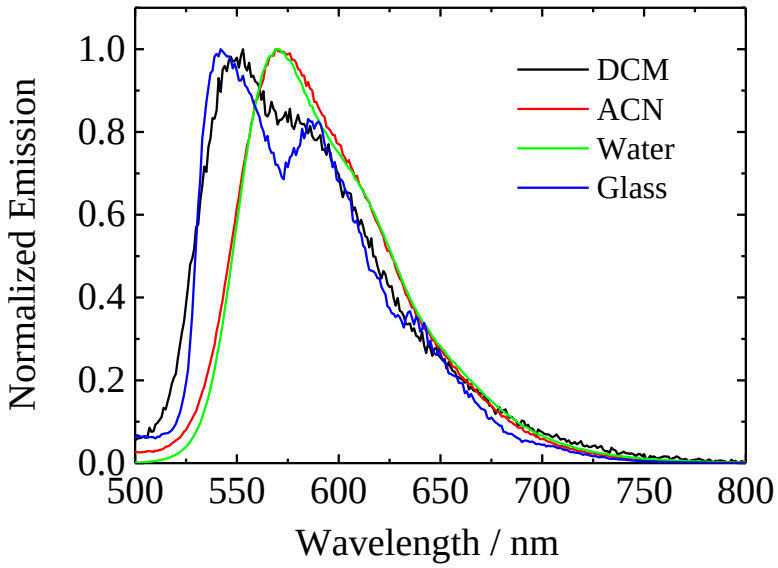

Figure S13. Emission spectra of complex **2** in degassed CH_2Cl_2 (black), CH_3CN (red), water (containing 1% PF127) (green) at 298 K, and alcoholic glass (EtOH:MeOH = 4:1, *v*/*v*) at 77 K (blue).

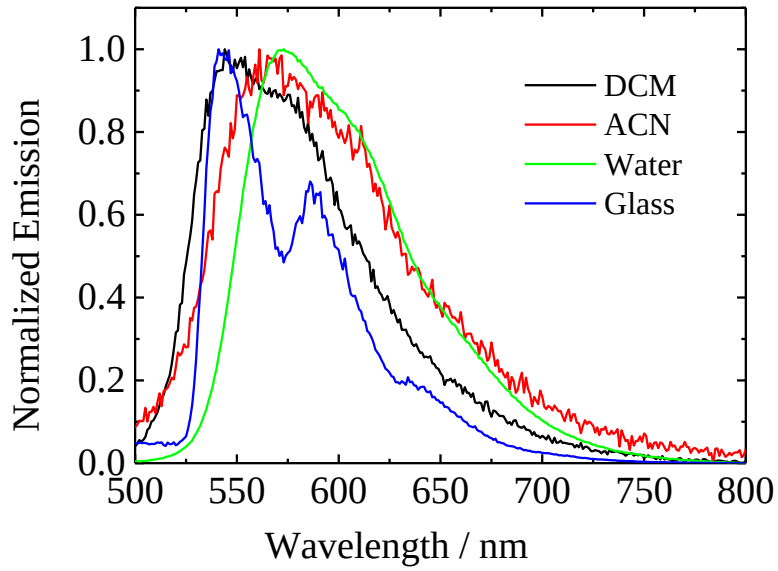

Figure S14. Emission spectra of complex **2a** in degassed CH_2Cl_2 (black), CH_3CN (red), water (green) at 298 K, and alcoholic glass (EtOH:MeOH = 4:1, *v*/*v*) at 77 K (blue).

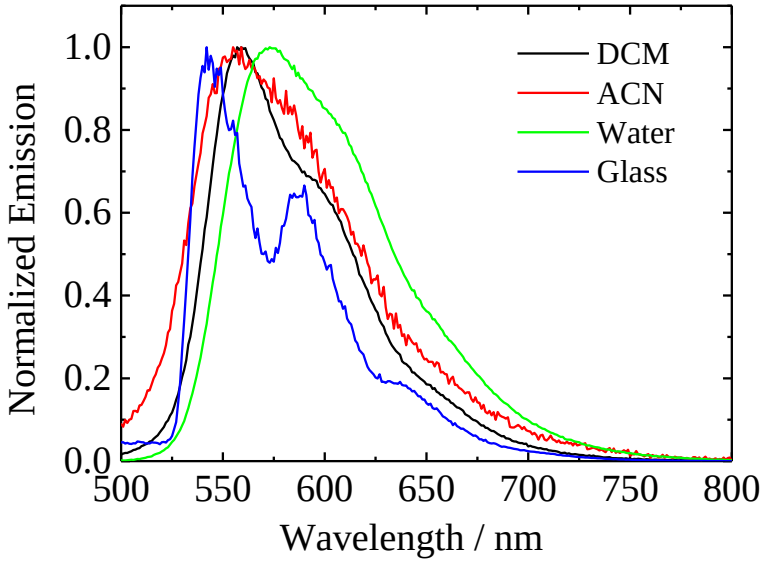

Figure S15. Emission spectra of complex **2b** in degassed CH_2Cl_2 (black), CH_3CN (red), water (green) at 298 K, and alcoholic glass (EtOH:MeOH = 4:1, *v*/*v*) at 77 K (blue).

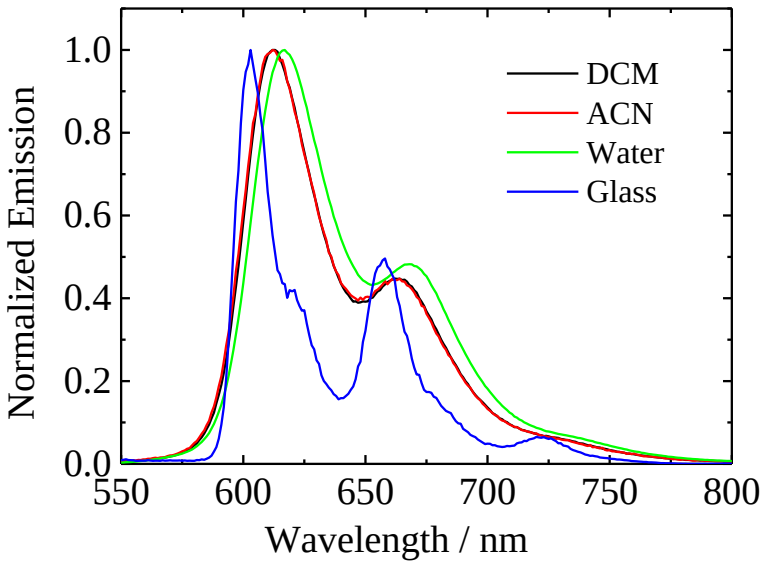

Figure S16. Emission spectra of complex **3** in degassed CH_2Cl_2 (black), CH_3CN (red), water (containing 1% PF127) (green) at 298 K, and alcoholic glass (EtOH:MeOH = 4:1, *v*/*v*) at 77 K (blue).

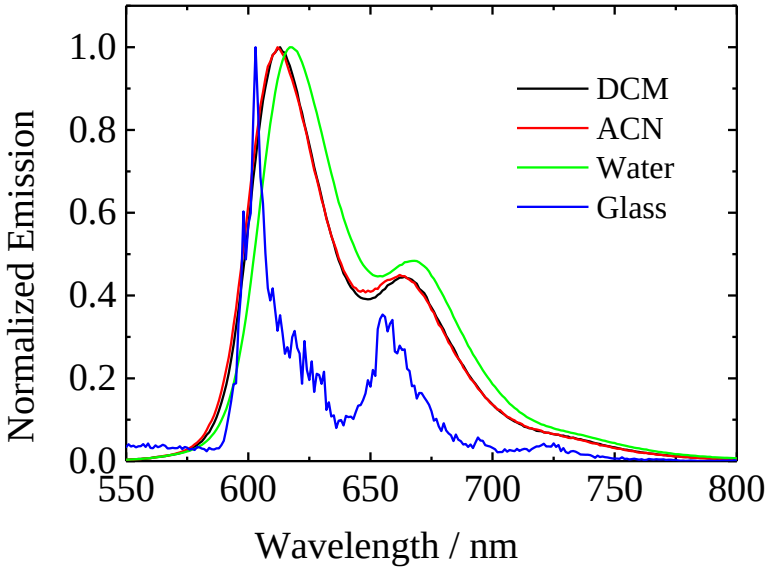

Figure S17. Emission spectra of complex **3a** in degassed CH_2Cl_2 (black), CH_3CN (red), water (green) at 298 K, and alcoholic glass (EtOH:MeOH = 4:1, *v*/*v*) at 77 K (blue).

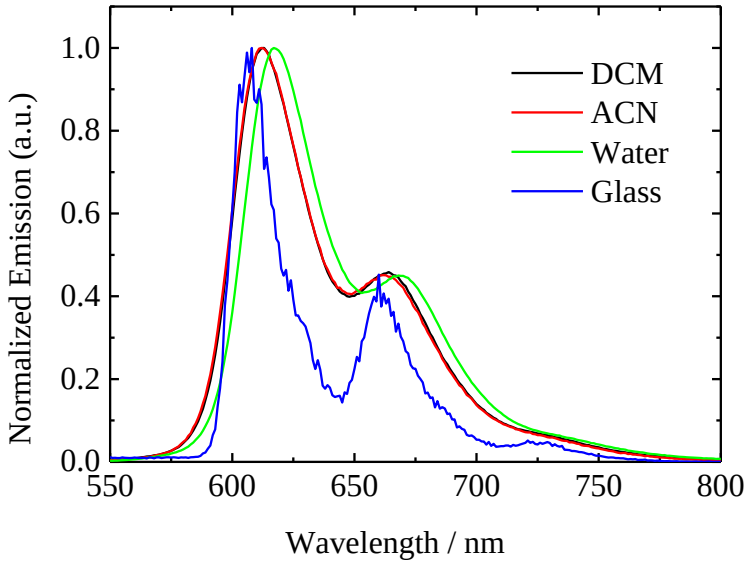

Figure S18. Emission spectra of complex **3b** in degassed CH_2Cl_2 (black), CH_3CN (red), water (green) at 298 K, and alcoholic glass (EtOH:MeOH = 4:1, *v*/*v*) at 77 K (blue).

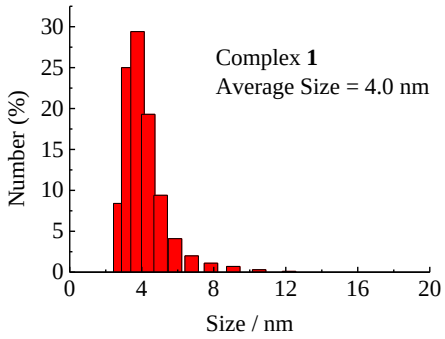
Complex 1
Average Size = 4.0 nm
Number (%)
Size / nm

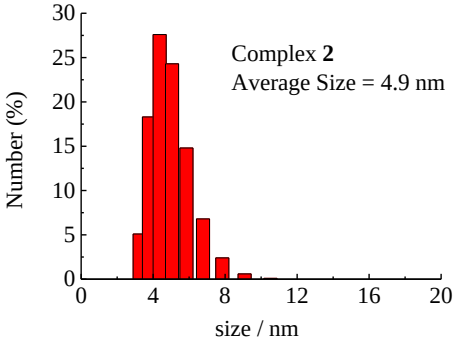
Complex 2
Average Size = 4.9 nm
Number (%)
size / nm

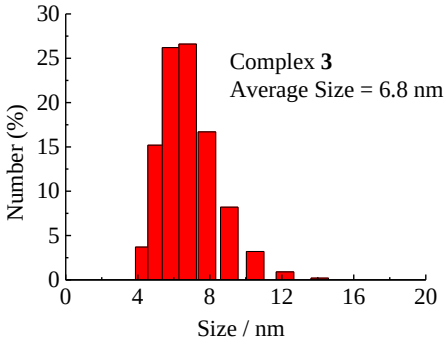
Complex 3
Average Size = 6.8 nm
Number (%)
Size / nm

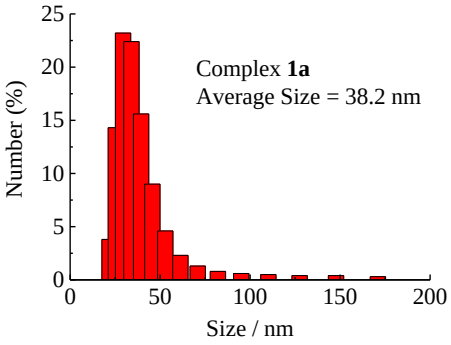
Complex 1a
Average Size = 38.2 nm
Number (%)
Size / nm

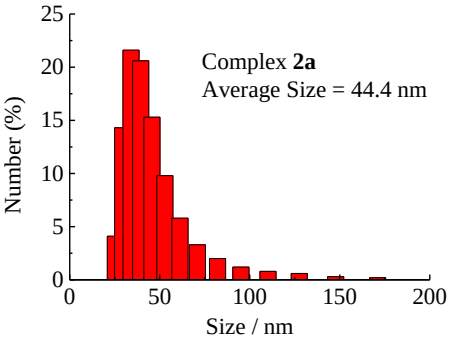
Complex 2a
Average Size = 44.4 nm
Number (%)
Size / nm

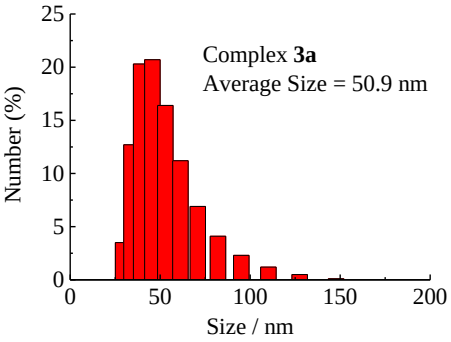
Complex 3a
Average Size = 50.9 nm
Number (%)
Size / nm

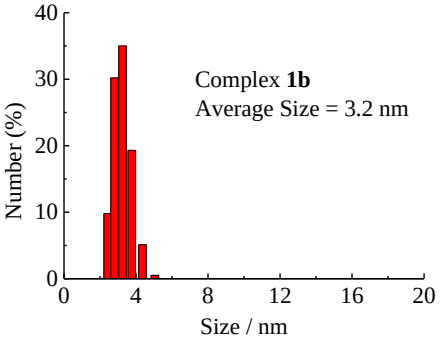
Complex 1b
Average Size = 3.2 nm
Number (%)
Size / nm

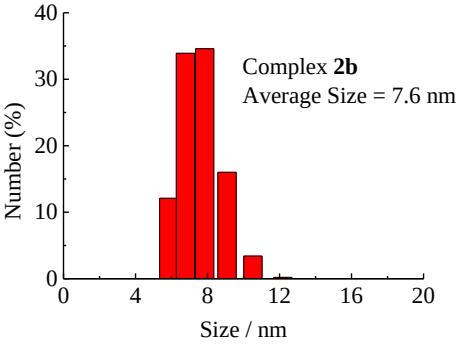
Complex 2b
Average Size = 7.6 nm
Number (%)
Size / nm

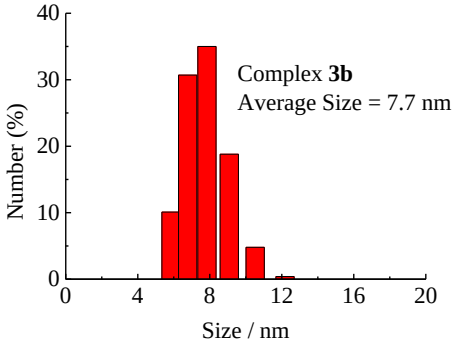

Figure S19. Dynamic Light Scattering (DLS) results of complexes **1** – **3** in 1% PF127 aqueous solution, complexes **1a** – **3a** in 1% aqueous CH_3CN, and complexes **1b** – **3b** in water.

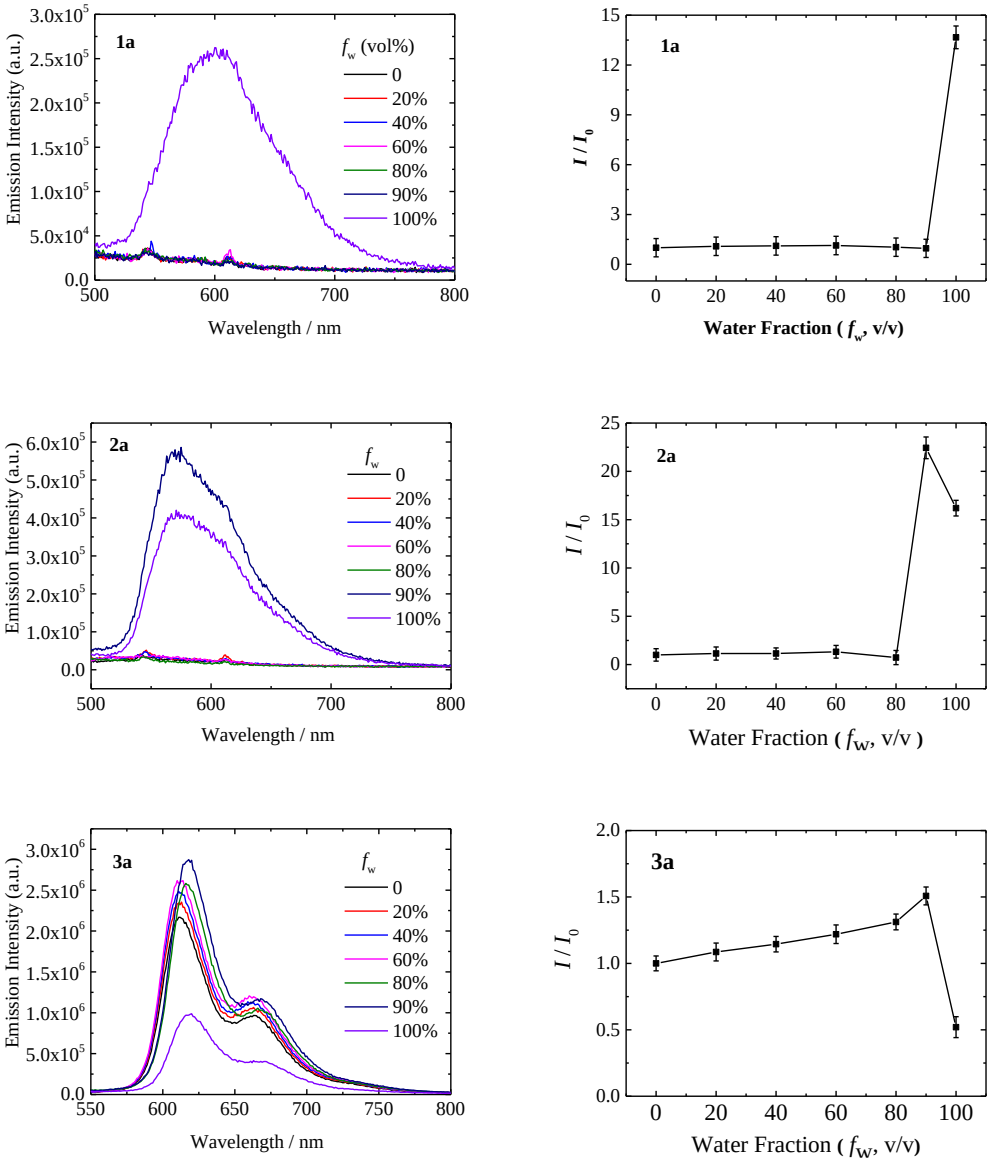

Figure S20. Emission spectra of complexes **1a** – **3a** in a mixture of CH_3CN and H_2O with various water fractions (f_w) at 298 K (the aqueous portion contained 1% PF127); λ_{ex} = 365 nm.

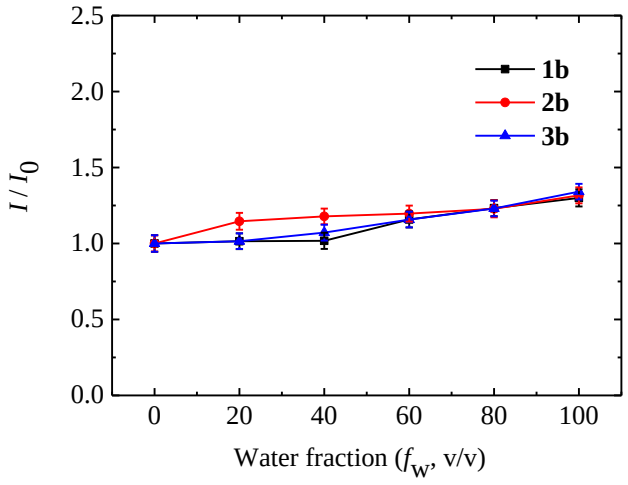

Figure S21. Relative emission intensities of complexes **1b** – **3b** in a mixture of CH_3CN and H_2O with various water fractions (f_w) at 298 K; λ_{ex} = 365 nm.

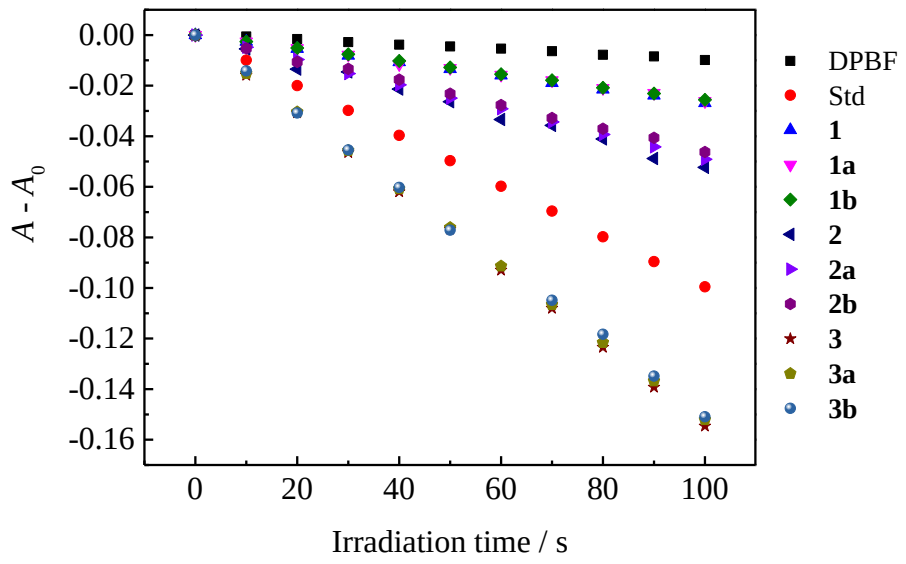

Figure S22. A plot of ($A - A_0$) of DPBF (10 μM) at 418 nm versus irradiation time in aerated CH_3CN in the presence of $[Ru(bpy)_3]Cl_2$ (circles), complexes **1** (up triangles), **1a** (down triangles), **1b** (diamonds), **2** (left triangles), **2a** (right triangles), **2b** (hexagons), **3** (stars), **3a** (pentagons), and **3b** (spheres) upon irradiation at 450 nm. A solution of DPBF without any sensitizer (cubes) was used as the negative control.

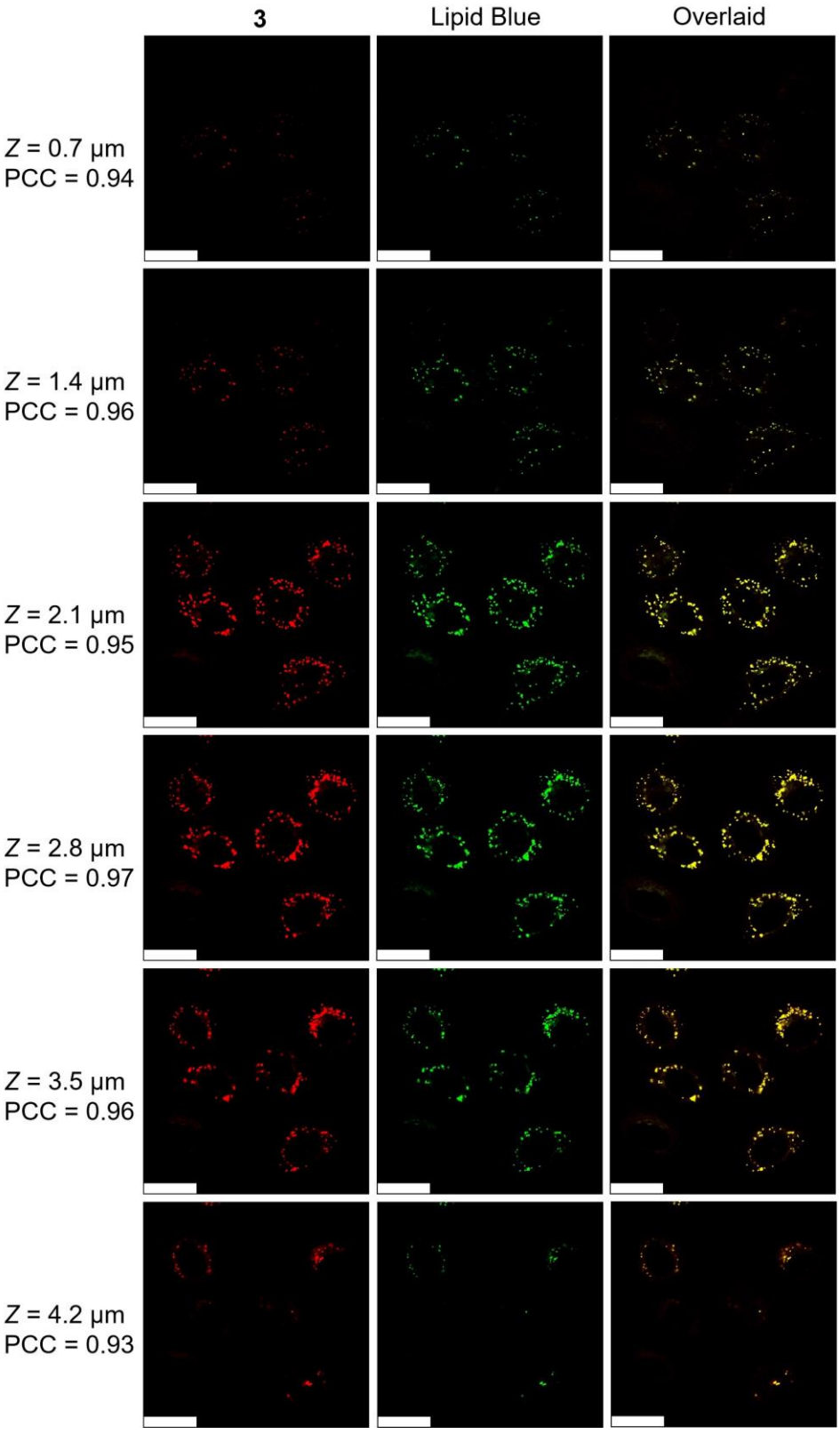

Figure S23. *Z*-stacks of LSCM images of HeLa cells labeled with complex **3** (10 μM, 1% PF127, λ_{ex} = 405 nm, emission: 550 – 700 nm) at 37 °C for 6 h. Scale bar: 25 μm.

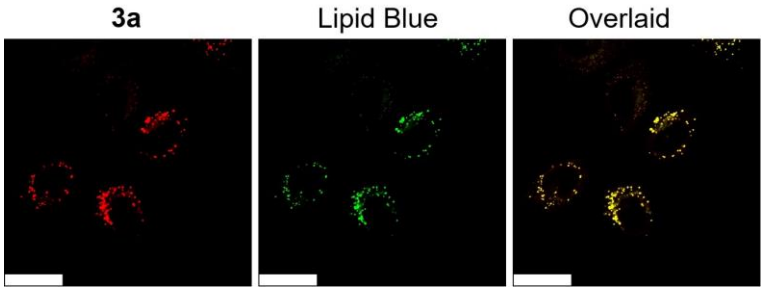

Figure S24. LSCM images of HeLa cells treated with complex **3a** (10 μM, 1% PF127, 6 h, λ_{ex} = 405 nm, emission: 550 – 700 nm) and Lipid Blue (1 μM, 15 min, λ_{ex} = 405 nm, emission: 415 − 495 nm) at 37°C. Scale bar: 25 μm.

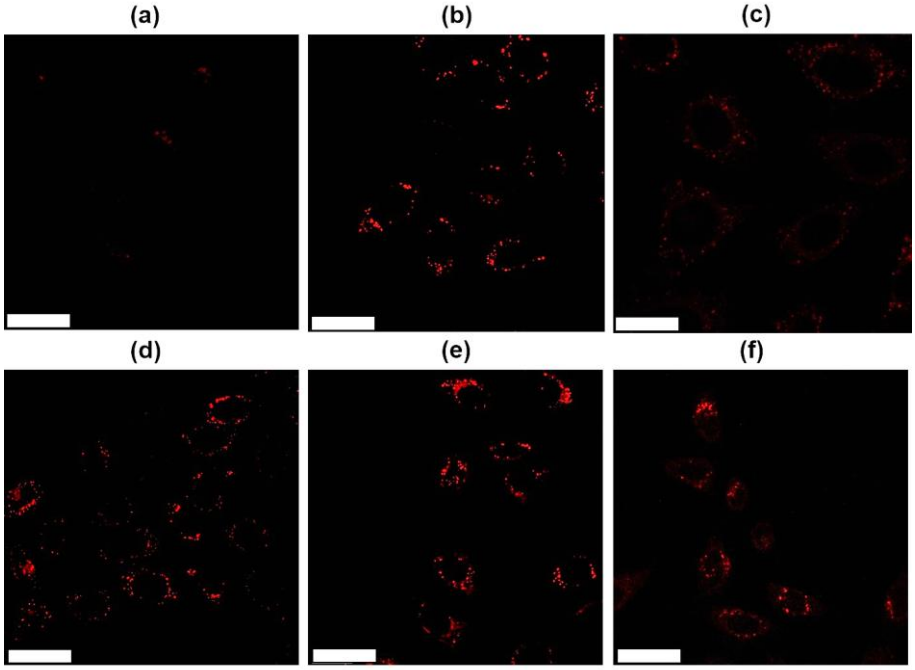

Figure S25. LSCM images of HeLa cells incubated with complex **3a** (10 μM, λ_{ex} = 405 nm, emission: 550 – 700 nm) at (a) 4℃ and (b) 37℃ for 6 h, or at 37 ℃ for 6 h after the cells had been preincubated with (c) β-cyclodextrin (5 mM), (d) chlorpromazine (μg mL^{-1}), (e) sucrose (0.3 M), and (f) colchicine (12.5 μM) for 2 h. Scale bar: 25 μm.

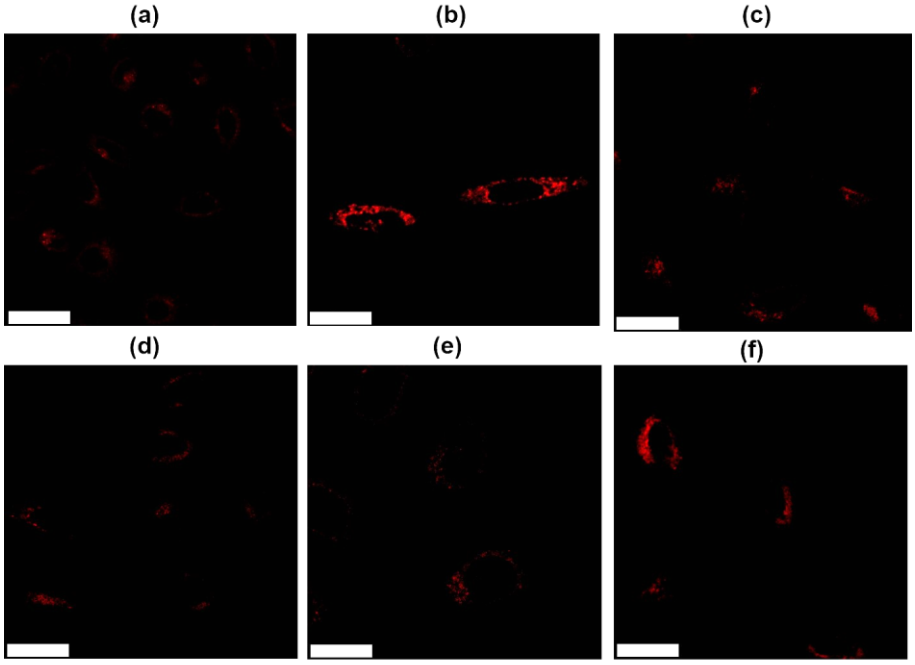

Figure S26. LSCM images of HeLa cells incubated with complex **3b** (10 μM, λ_{ex} = 405 nm, emission: 550 – 700 nm) at (a) 4℃ and (b) 37℃ for 6 h, or at 37 ℃ for 6 h after the cells had been preincubated with (c) β-cyclodextrin (5 mM), (d) chlorpromazine (10 μg mL^{-1}), (e) sucrose (0.3 M), and (f) colchicine (12.5 μM) for 2 h. Scale bar: 25 μm.

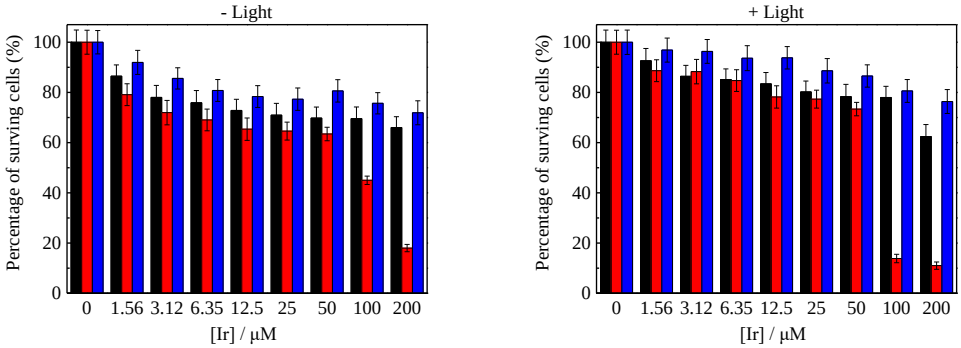

Figure S27. Viability of HeLa cells treated with complexes **1** (black), **1a** (red), and **1b** (blue) in the dark for 24 h. The cells were further incubated in the dark or irradiated at 450 nm (5 mW cm^{-2}) for 5 min, and subsequently incubated in the dark for 24 h.

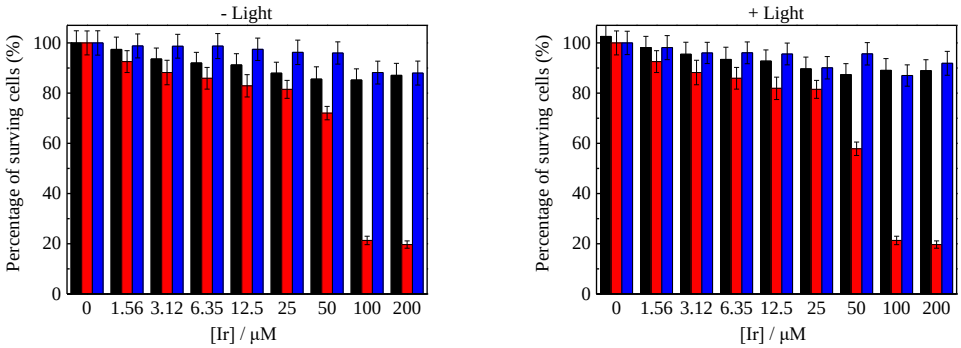

Figure S28. Viability of HeLa cells treated with complexes **2** (black), **2a** (red), and **2b** (blue) in the dark for 24 h. The cells were further incubated in the dark or irradiated at 450 nm (5 mW cm^{-2}) for 5 min, and subsequently incubated in the dark for 24 h.

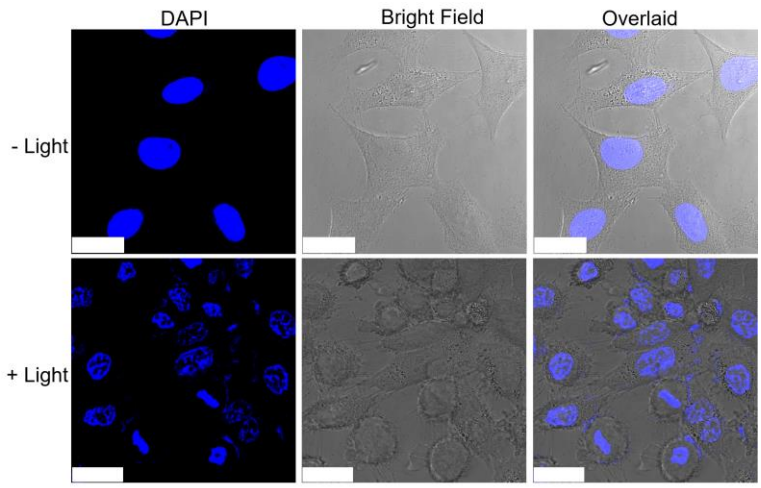

Figure S29. Changes of nucleus morphology in HeLa cells pretreated with the POSS complex **3** (10 μM, 1% PF127, 12 h) without (upper) or with (lower) light irradiation at 450 nm for 5 min, fixed with 4% paraformaldehyde in PBS for 15 min, and stained with DAPI (10 μM, 15 min, λ_{ex} = 405 nm, emission: 415 − 495 nm). Scale bar: 25 μm.

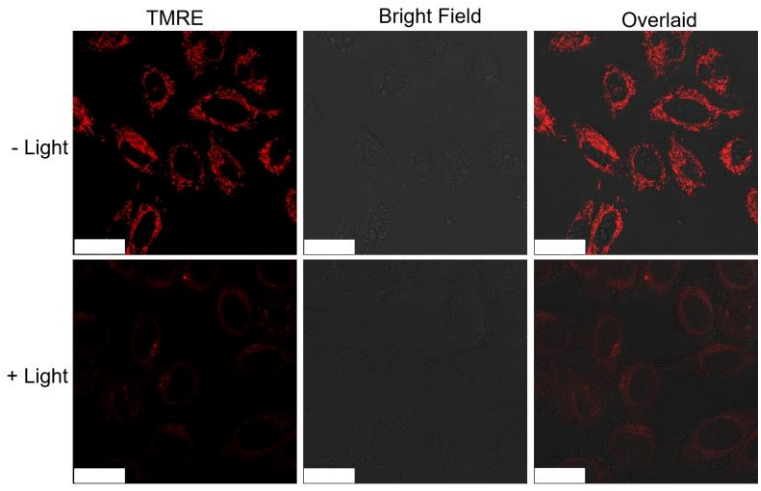

Figure S30. Changes of mitochondrial membrane potential (MMP) in HeLa cells pretreated with the POSS complex **3** (10 μM, 1% PF127, 12 h) without (upper) or with (lower) irradiation at 450 nm for 5 min, and stained with TMRE (10 μM, 15 min, λ_{ex} = 488 nm, emission: 500 − 550 nm). Scale bar: 25 μm.

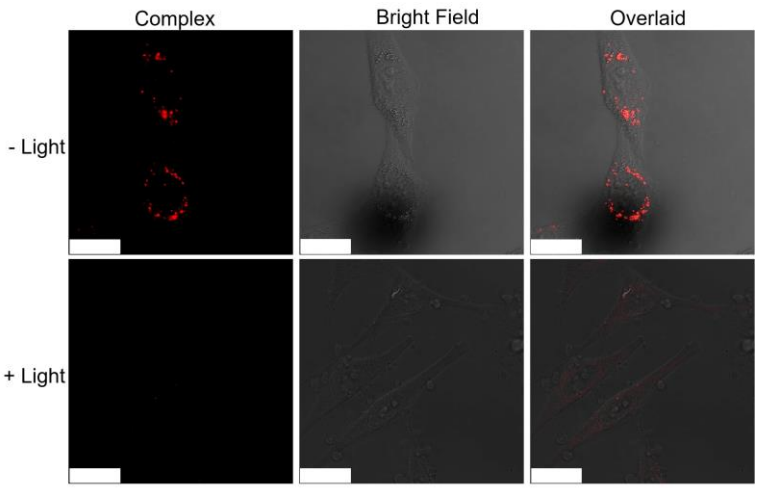

Figure S31. Changes of lipid droplets emission in HeLa cells pretreated with the POSS complex **3** (10 μM, 1% PF127, 12 h) without (upper) or with (lower) light irradiation at 450 nm for 5 min (λ_{ex} = 405 nm, emission: 550 − 700 nm) Scale bar: 25 μm.

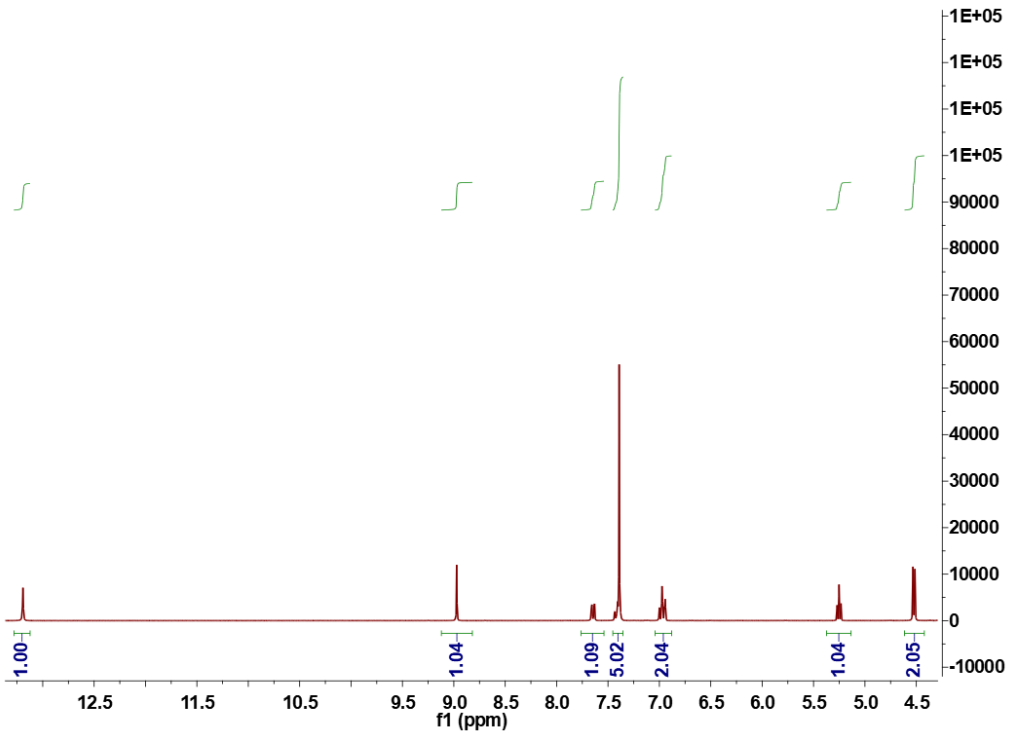

Figure S32. ^{1}H NMR spectrum of HL1 in DMSO-d_6.

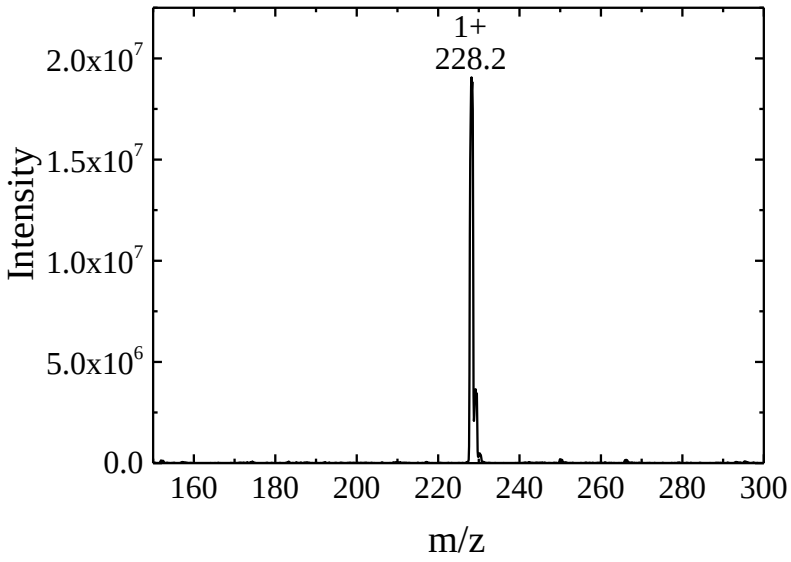

Figure S33. ESI-MS spectrum of HL1 in CH_3OH.

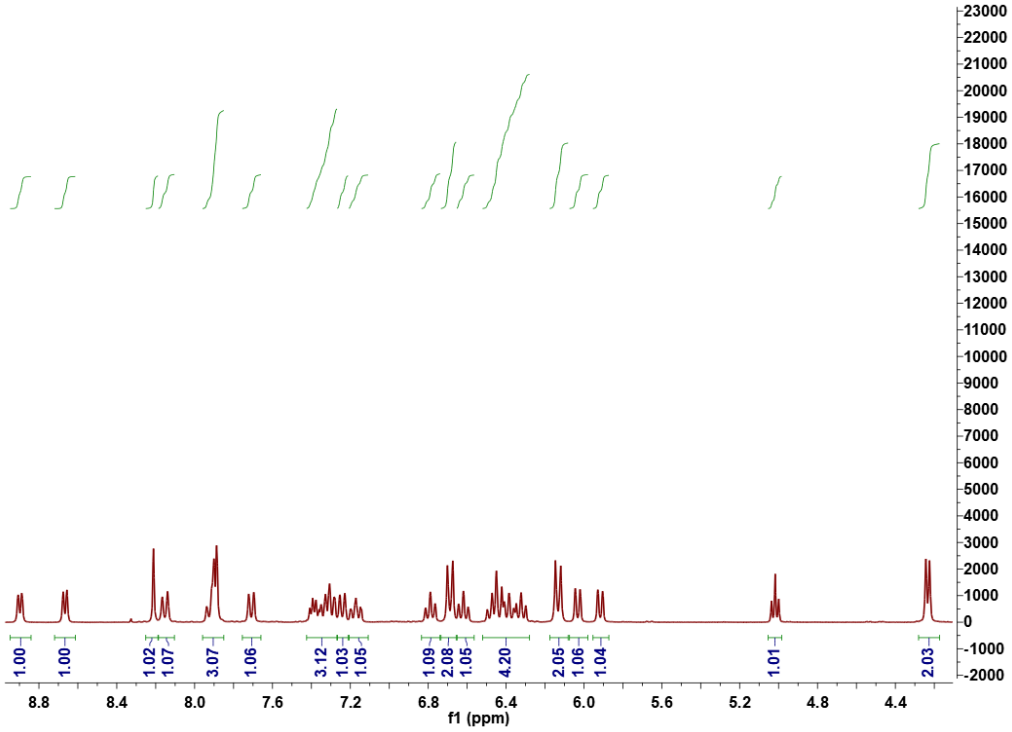

Figure S34. ^{1}H NMR spectrum of complex **1a** in DMSO-d_6.

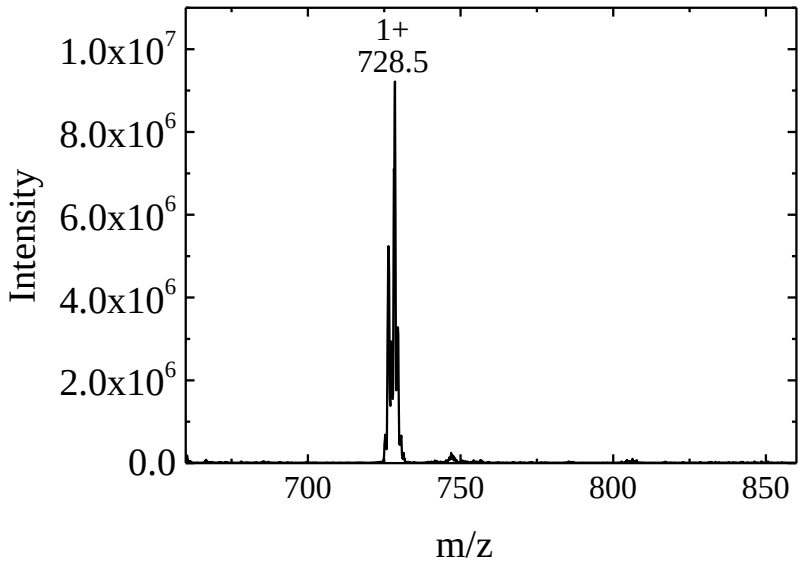

Figure S35. ESI-MS spectrum of complex **1a** in CH_3OH.

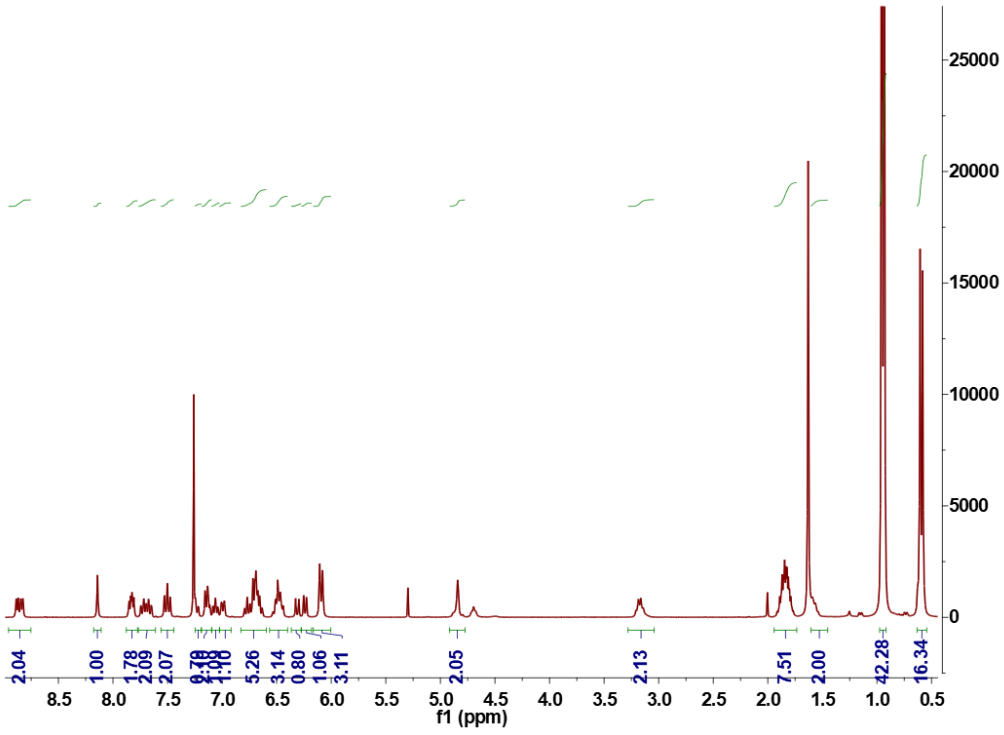

Figure S36. ^1H NMR spectrum of complex **1** in $CDCl_3$.

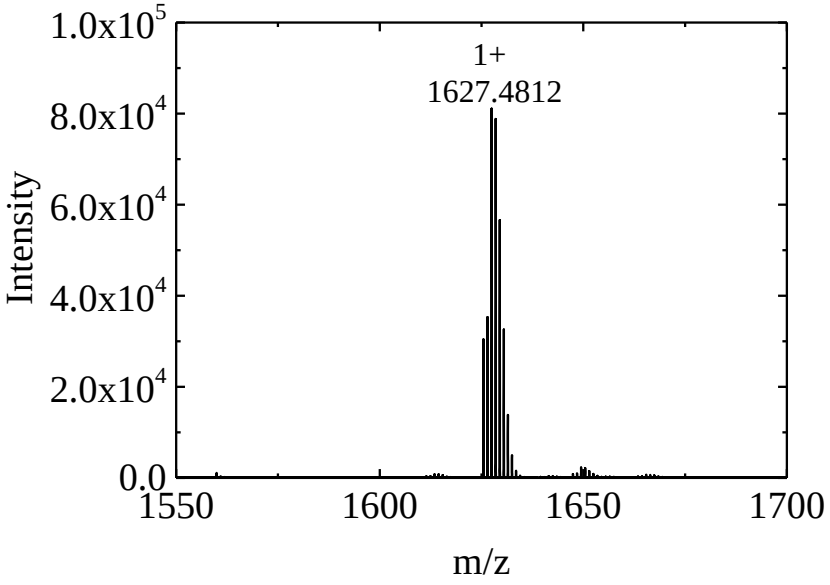

Figure S37. ESI-MS spectrum of complex **1** in CH_3CN.

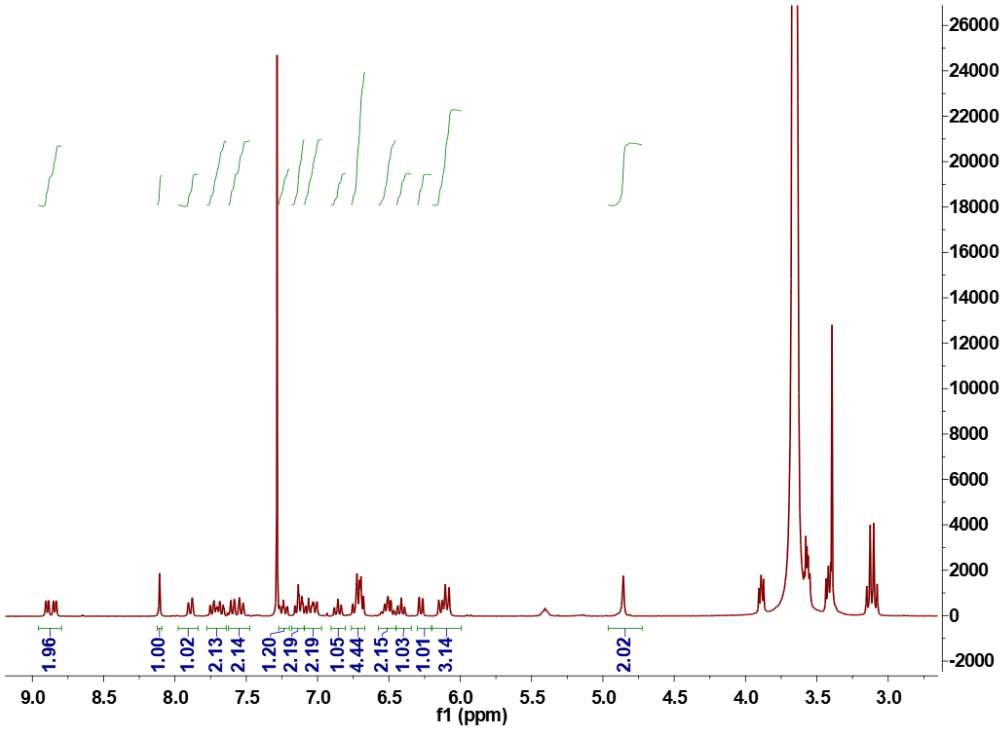

Figure S38. ^1H NMR spectrum of complex **1b** in $CDCl_3$.

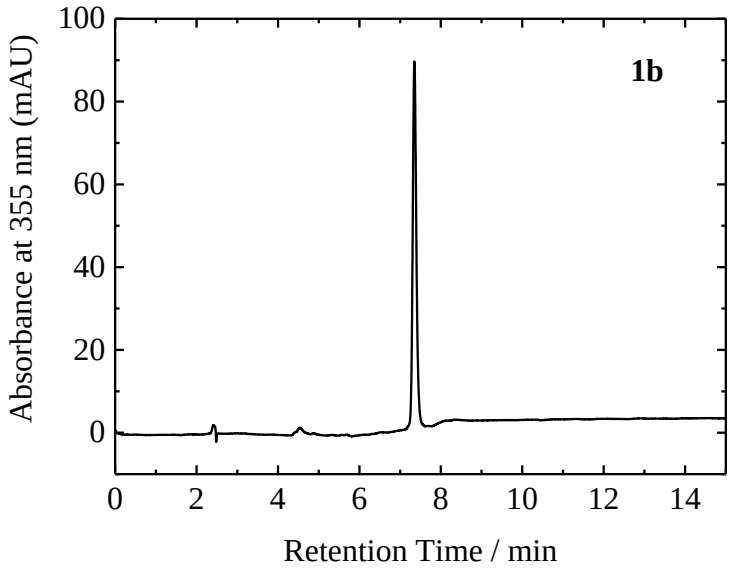

Figure S39. HPLC chromatogram of complex **1b** using CH_3OH as the mobile phase. The reverse-phase separation was performed on a C18 column (ZORBAX Eclipse Plus C18, 4.6 × 150 mm, 5 μm) (flow rate: 4.0 mL min^{-1}). Detector: UV (350 nm).

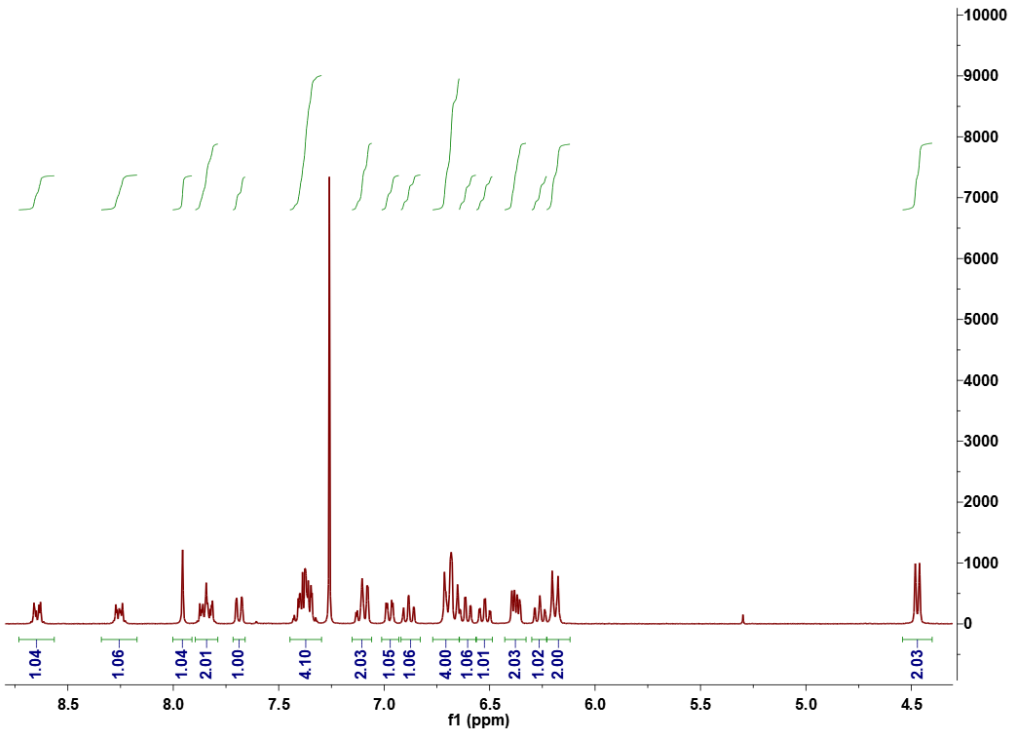

Figure S40. ^1H NMR spectrum of complex **2a** in $CDCl_3$.

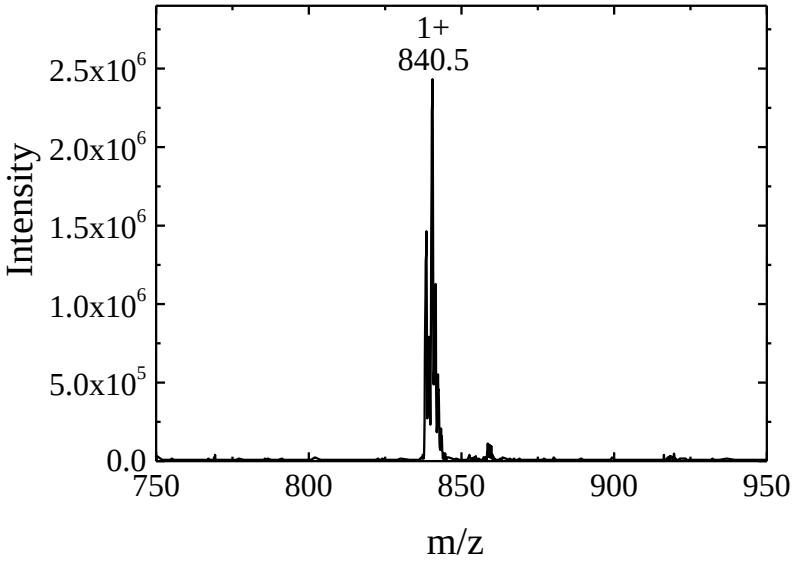

Figure S41. ESI-MS spectrum of complex **2a** in CH_3OH.

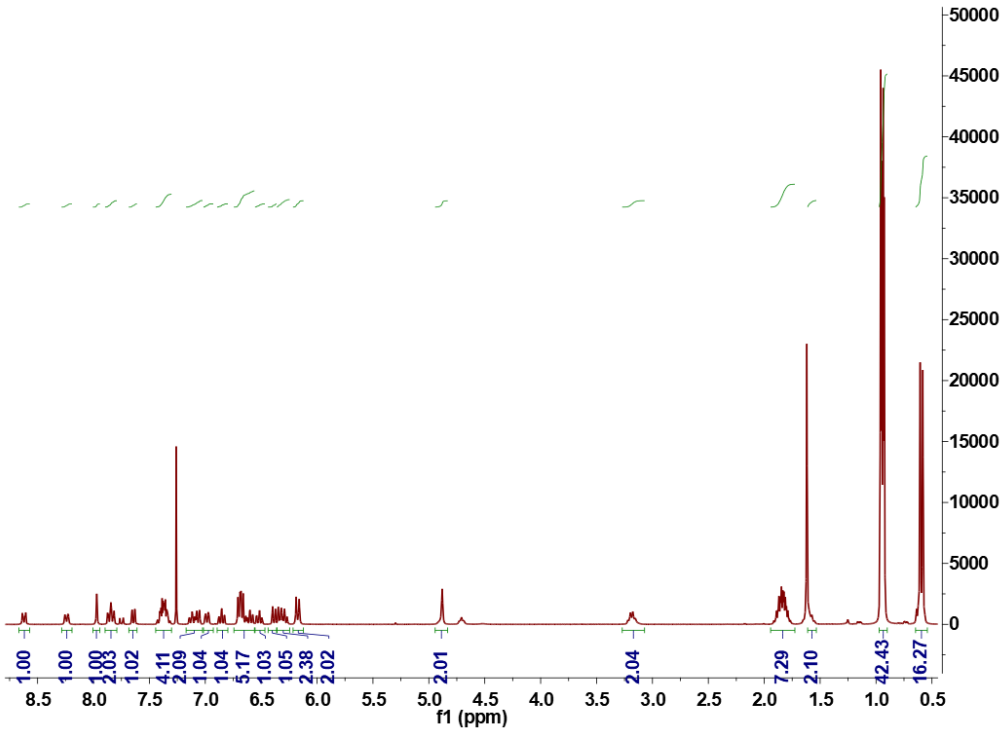

Figure S42. ^1H NMR spectrum of complex **2** in $CDCl_3$.

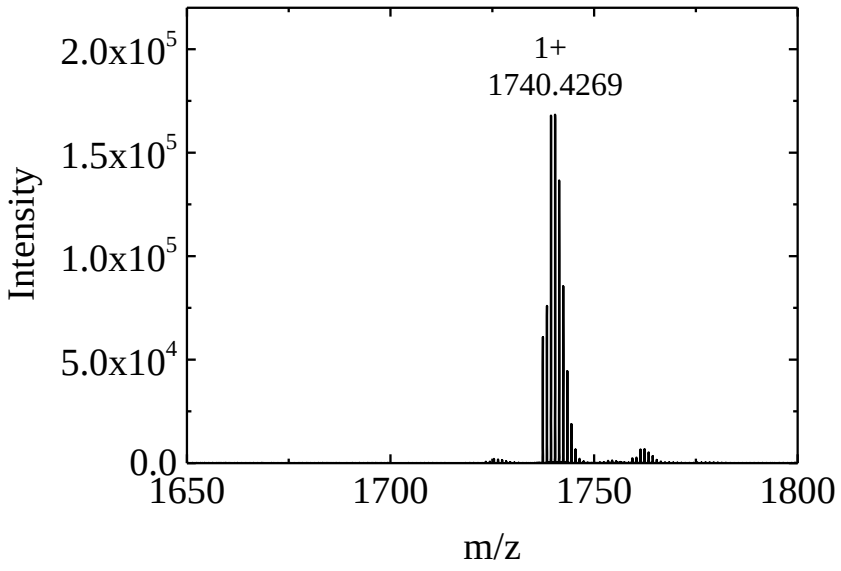

Figure S43. ESI-MS spectrum of complex **2** in CH_3CN.

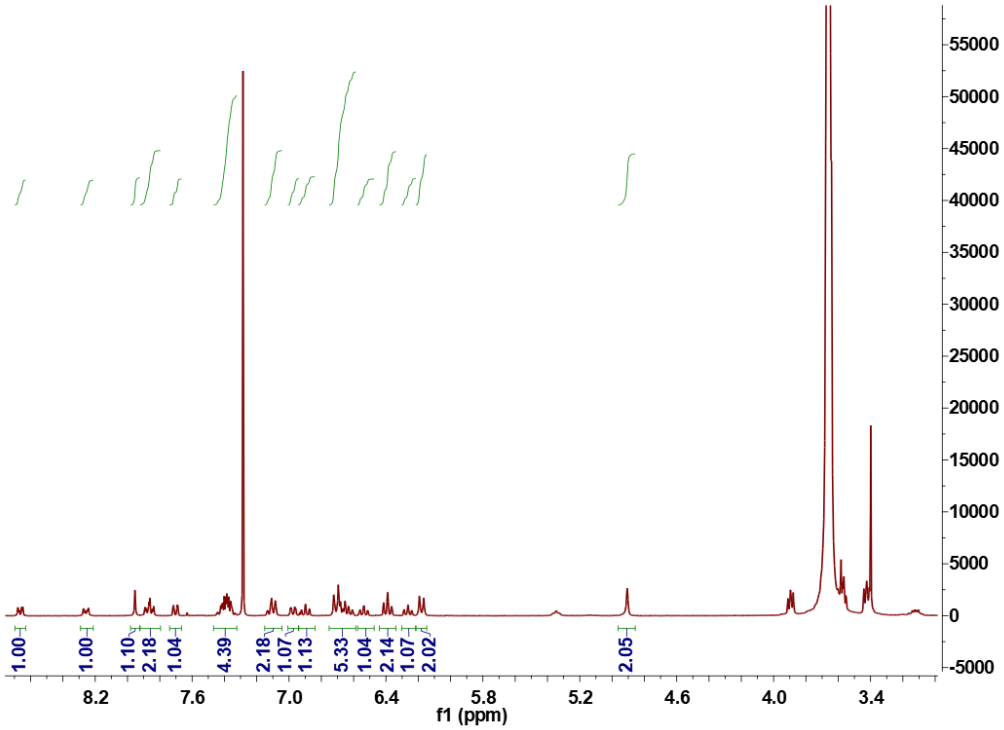

Figure S44. ^1H NMR spectrum of complex **2b** in $CDCl_3$.

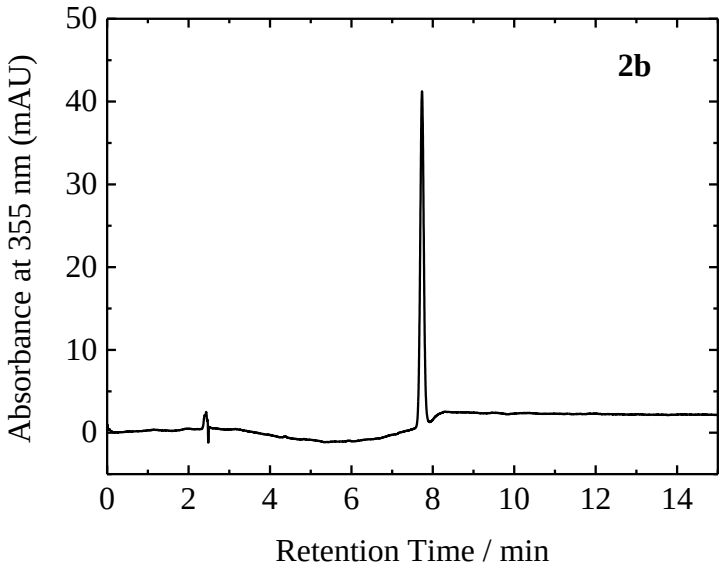

Figure S45. HPLC chromatogram of complex **2b** using CH_3OH as the mobile phase. The reverse-phase separation was performed on a C18 column (ZORBAX Eclipse Plus C18, 4.6 × 150 mm, 5 μm) (flow rate: 4.0 mL min^{-1}). Detector: UV (350 nm).

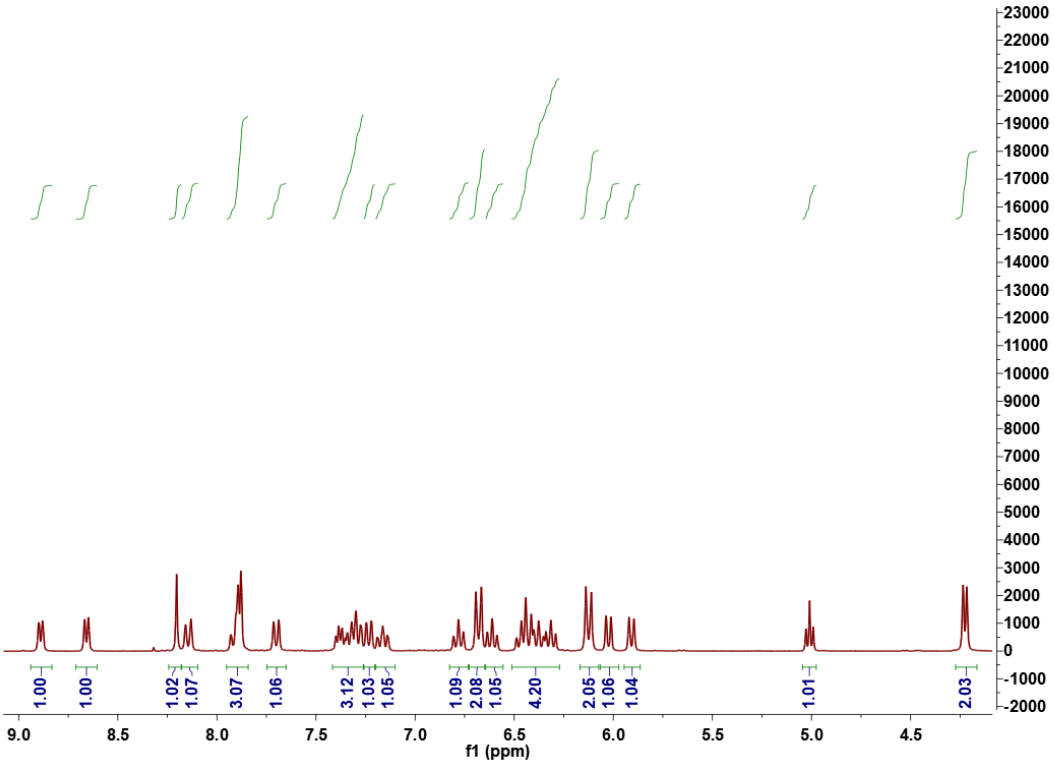

Figure S46. ^1H NMR spectrum of complex **3a** in DMSO-d_6.

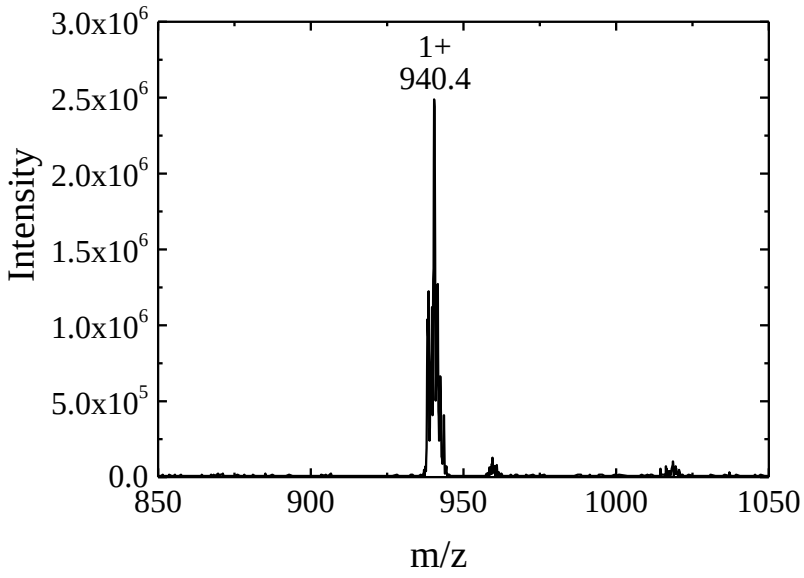

Figure S47. ESI-MS spectrum of complex **3a** in CH_3OH.

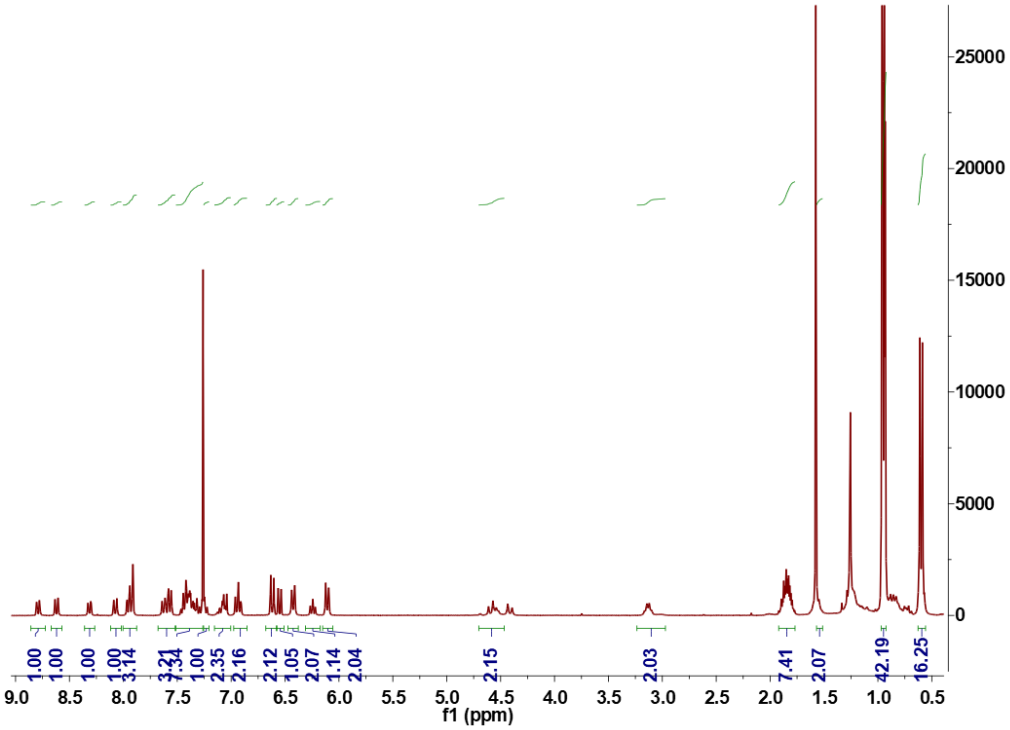

Figure S48. ^1H NMR spectrum of complex **3** in $CDCl_3$.

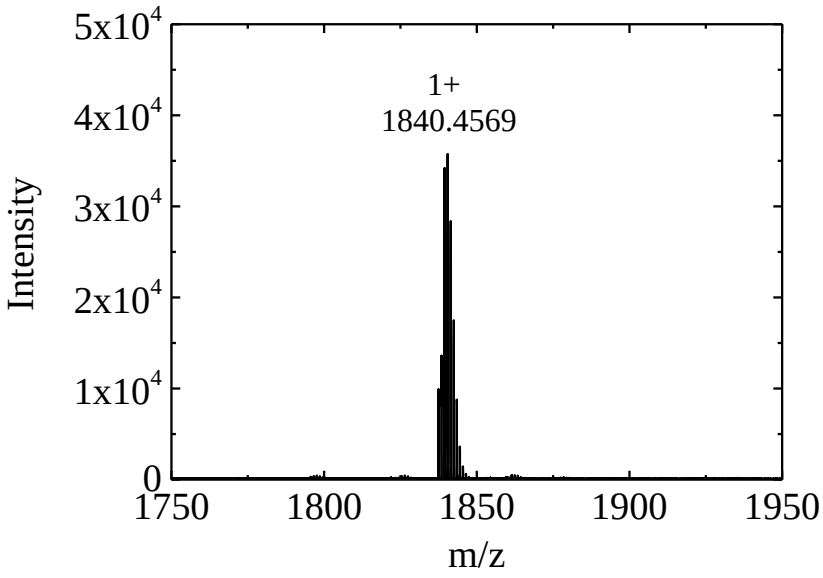

Figure S49. ESI-MS spectrum of complex **3** in CH_3CN.

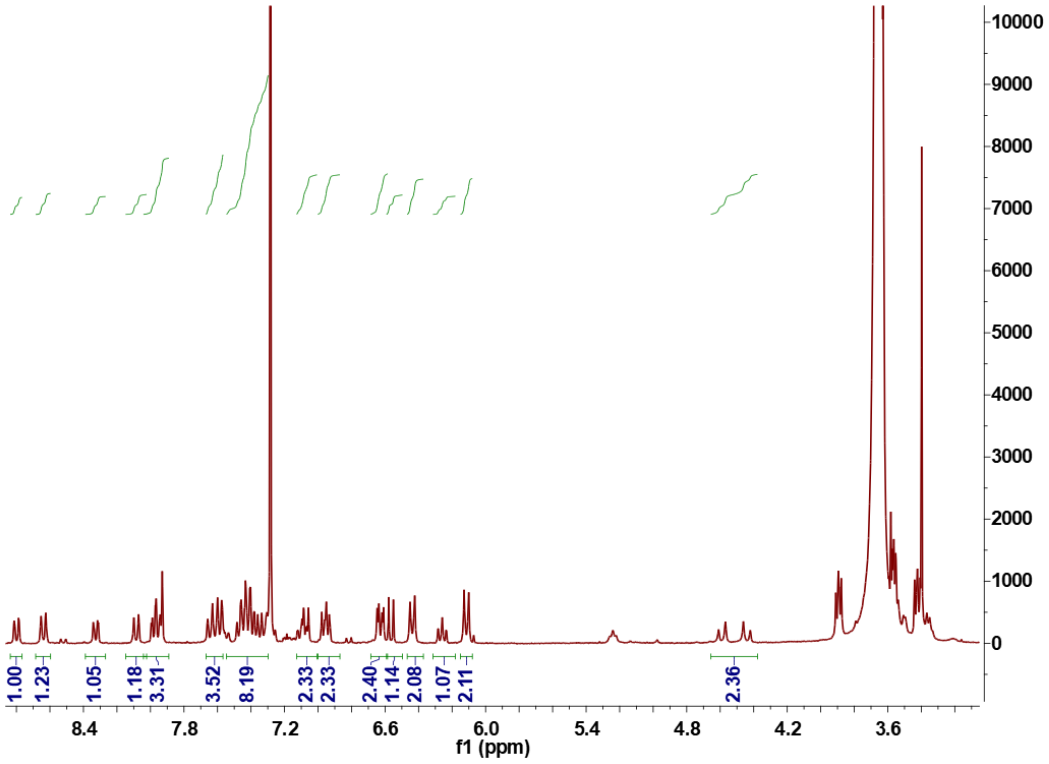

Figure S50. ^1H NMR spectrum of complex **3b** in $CDCl_3$.

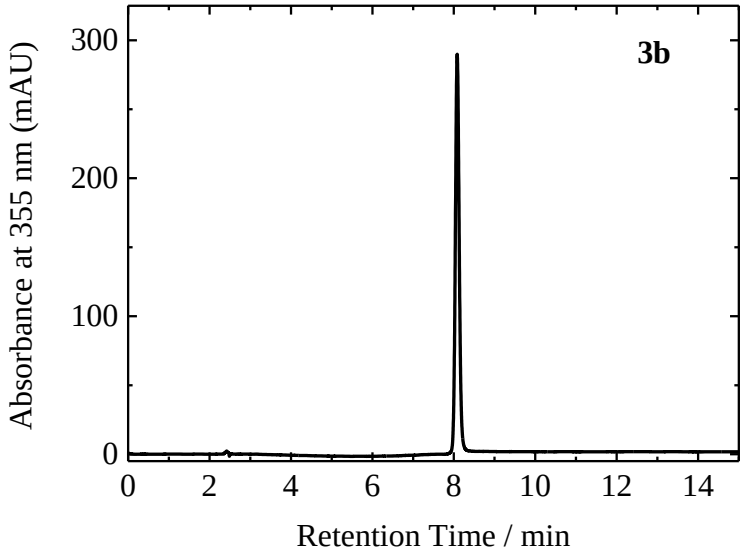

Figure S51. HPLC chromatogram of complex **3b** using CH_3OH as the mobile phase. The reverse-phase separation was performed on a C18 column (ZORBAX Eclipse Plus C18, 4.6 × 150 mm, 5 μm) (flow rate: 4.0 mL min^{-1}). Detector: UV (350 nm).

References

(1) Deligeorgiev, T. G. An improved method for the preparation of 2-aryl-, 2-hetaryl-and 2-styrylbenzothiazoles. *Dyes Pigm.* **1990**, *12*, 243.

(2) Garces, F. O.; King, K. A.; Watts, R. J. Synthesis, structure, electrochemistry, and photophysics of methyl-substituted phenylpyridine ortho-metalated iridium(III) complexes. *Inorg. Chem.* **1988**, *27*, 3464.

(3) Perrin, D. R.; Armarego, W. L. F. Purification of Laboratory Chemicals, Pergamon, Oxford (**1988**).

(4) Zhang, X.; Jackson, J. K.; Burt, H. M. Development of amphiphilic diblock copolymers as micellar carriers of taxol. *Int. J. Pharm.* **1996**, *132*, 195.

(5) Hackley, V. A.; Clogston. J. D. Characterization of Nanoparticles Intended for Drug Delivery, ed. S. E. McNeil, Humana Press, New York, NY, USA, **2011**, vol. 697, pp. 35 – 52.

(6) Demas, J. N.; Crosby, G. A. Measurement of photoluminescence quantum yields. A review. *J. Phys. Chem.* **1971**, *75*, 991.

(7) Suzuki, K.; Kobayashi, A.; Kaneko, S.; Takehira, K.; Yoshihara, T.; Ishida, H.; Shiina, Y.; Oishi, S.; Tobita, S. Reevaluation of absolute luminescence quantum yields of standard solutions using a spectrometer with an integrating sphere and a back-thinned CCD detector. *Phys. Chem. Chem. Phys.* **2009**, *11*, 9850.

(8) Li, S. P.-Y.; Lau, C. T.-S.; Louie, M.-W.; Lam, Y.-W.; Cheng, S. H.; Lo, K. K.-W. Mitochondria-targeting cyclometalated iridium(III)–PEG complexes with tunable photodynamic activity. *Biomaterials* **2013**, *34*, 7519.

(9) Abdel-Shafi, A. A.; Beer, P. D.; Mortimer R. J.; Wilkinson, F. Photosensitized generation of singlet oxygen from vinyl linked benzo-crown-ether−bipyridyl ruthenium (II) complexes. *J. Phys. Chem. A* **2000**, *104*, 192.

(10) https://www.atcc.org/products/all/htb-22.aspx#culturemethod

(11) Ferrara, M. A.; Filograna, A.; Ranjan, R.; Corda, D.; Valente, C.; Sirleto, L. Three-dimensional label-free imaging throughout adipocyte differentiation by stimulated Raman microscopy. *Plos One* **2019**, *14*, e0216811.

(12) Zhang, F.; Liu, Y.; Yang, B.; Wen, G.; Liu, B. Near-infrared AIEgens for lipid droplets imaging in corpus adiposum or trachea of Locusta migratoria and its application in photodynamic therapy. *Sens. Actuators B* **2020**, *322*, 128589.

(13) Yip, A. M.-H.; Shum, J.; Liu, H.-W.; Zhou, H.; Jia, M.; Niu, N.; Li, Y.; Yu, C.; Lo, K. K.-W. Luminescent Rhenium(I) – Polypyridine Complexes Appended with a Perylene Diimide or Benzoperylene Monoimide Moiety: Photophysics, Intracellular Sensing, and Photocytotoxic Activity. *Chem. Eur. J.* **2019**, 25, 8970.

(14) Indrigo, E.; Clavadetscher, J.; Chankeshwara, S. V.; Megia-Fernandez, A.; Lilienkampf, A.; Bradley, M. Intracellular delivery of a catalytic organometallic complex. *Chem. Commun.* **2017**, *53*, 6712.

(15) Adarsh, N.; Babu, P. S. S.; Avirah, R. R.; Viji, M.; Nair, S. A.; Ramaiah, D. Aza-BODIPY nanomicelles as versatile agents for the in vitro and in vivo singlet oxygen-triggered apoptosis of human breast cancer cells. *J. Mater. Chem. B* **2019**, *7*, 2372.

(16) Sudheesh, K. V.; Jayaram, P. S.; Samanta, A.; Bejoymohandas, K. S.; Jayasree, R. S.; Ajayaghosh, A. A Cyclometalated Ir^{III} Complex as a Lysosome-Targeted Photodynamic Therapeutic Agent for Integrated Imaging and Therapy in Cancer Cells. *Chem. Eur. J.* **2018**, *24*, 10999.

(17) Takahashi, M.; Shibata, M.; Niki, E. Estimation of lipid peroxidation of live cells using a fluorescent probe, diphenyl-1-pyrenylphosphine. *Free Radical Bio. Med.* **2001**, *31*, 164.